Chapter 3
Orientation Effects and Anisotropy of Properties in 2–2 and Related Composites

The 2–2 connectivity pattern of a composite [1–3] is a structure where there are two types of layers which are alternating in a certain direction. The 2–2 composite family is characterised by a laminar structure wherein two components are continuously distributed along two axes of a rectangular co-ordinate system $(X_1X_2X_3)$. Each component is present in the separate layer. The relative simplicity of the 2–2 composite structure and the possibility of varying the volume fractions of the components in a wide range allow the manufacture and design of the 2–2 composite with tailored (e.g., extreme) values of its effective parameters. Methods suitable for manufacturing these widespread 2–2 FC/polymer composites are discussed in a series of review papers (see, for instance, papers [3–5]).

The 2–2 FC/polymer composites are usually manufactured in two modifications (Fig. 3.1), namely, as composites with a series connection and a parallel connection of adjacent layers [1, 2]. In the series-connectied composite sample the C1 and C2 layers are alternating in the OX_3 direction (Fig. 3.1a) and interfaces are perpendicular to OX_3, and this co-ordinate axis is the poling axis. In the parallel-connected composite the poling axis OX_3 is parallel to the interfaces that separate the C1 and C2 layers (Fig. 3.1b). It is obvious that these two modifications are characterised by different electromechanical properties [2] and anisotropy with respect to the poling axis OX_3. In the series-connected composite the piezoelectric coefficients d^*_{3j} concerned with the poling axis obey the condition $d^*_{31} = d^*_{32} \neq d^*_{33}$, while the parallel-connected composite is characterised by an inequality $d^*_{31} \neq d^*_{32} \neq d^*_{33}$ [2].

The 2–2 composite architecture is of value due to a particular non-monotonic volume-fraction dependence of their effective parameters. For instance, the series-connected 2–2 composite based on the Pb(Zr, Ti)O_3-type FC is characterised by several types of the volume-fraction dependence [6, 7] of the thickness ECF $k^*_t = e^*_{33}/(c^{*D}_{33}\varepsilon^{*\xi}_{33})^{1/2}$ [see also Eq. (1.25)], maxima of the piezoelectric coefficient e^*_{31} and dielectric permittivity $\varepsilon^{*\sigma}_{11}$ and a strong dependence of k^*_t, e^*_{31}, $\varepsilon^{*\sigma}_{11}$, and other parameters on the ratio between the elastic moduli of the individual components [8]. Moreover, the piezoelectric coefficient e^*_{31} of the series-connected composite [9] can pass through a zero value and reach max $e^*_{31} > 0$, although both the

V. Yu. Topolov et al., *Piezo-Active Composites*,
Springer Series in Materials Science 185, DOI: 10.1007/978-3-642-38354-0_3,

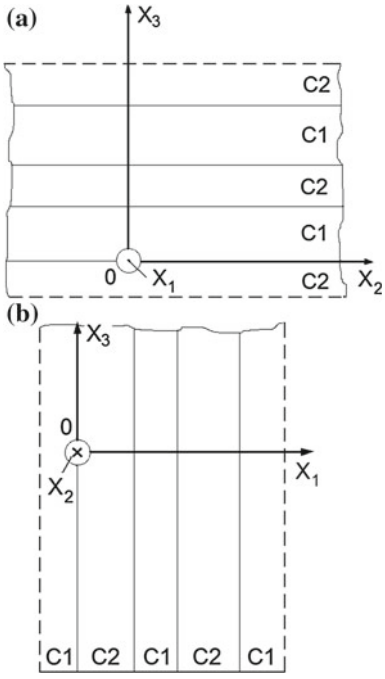

Fig. 3.1 Schematic of the 2–2 series-connected (**a**) and parallel-connected (**b**) composites with components denoted as C1 and C2. $(X_1X_2X_3)$ is the rectangular co-ordinate system

components ($n = 1$ and 2, i.e., C1 and C2 layers in Fig. 3.1a) have negative values of the piezoelectric coefficient $e_{31}^{(n)}$. A squared strain–voltage figure of merit

$$(Q_{33}^*)^2 = d_{33}^* g_{33}^* \tag{3.1}$$

exhibits a maxima [10] when varying the volume fraction of the FC component in a 2–2 series-connected composite. The parallel-connected 2–2 composite based on Pb(Zr, Ti)O_3-type FC exhibits a non-monotonic behaviour of the thickness ECF k_t^* and the hydrostatic (or hydrophone) piezoelectric coefficients [11, 12]

$$d_h^* = d_{33}^* + d_{32}^* + d_{31}^* \text{ and } g_h^* = g_{33}^* + g_{32}^* + g_{31}^*. \tag{3.2}$$

In this chapter we will discuss features of the performance of 2–2 and related composites based on either a FC or SC by taking into account the orientation effect and the anisotropy of the effective properties of these composites.

3.1 Ceramic/Polymer Composites: An Effect of the Orientation of the Remanent Polarisation Vector on the Piezoelectric Anisotropy

The first results on the performance of oriented 2–2 composites based on a "soft" PZT FC were published in work [3, 13]. The orientation angle of the remanent polarisation vector $\boldsymbol{P}_r^{(1)}$ in the FC layers with respect to the poling direction of the composite was varied from 0° to 75°. The maximum of the squared hydrostatic figure of merit

$$(Q_h^*)^2 = d_h^* g_h^* \tag{3.3}$$

in the oriented 2–2 composite [13] is achieved by varying the orientation angle and volume fraction of the FC component. Equation (3.3) comprises the hydrostatic piezoelectric coefficients d_h^* and g_h^* from (3.2). The sumations in (3.2) characterise the hydrostatic response of a piezo-active element with electrodes that are perpendicular to the OX_3 axis.

In this section we consider examples of the volume-fraction and orientation dependence of the piezoelectric properties and their anisotropy factors in 2–2 FC/polymer composites. Among the vast group of FCs (see Table 1.2) we choose two compositions. The first composition is a "soft" PCR-7M FC with high values of piezoelectric coefficients $|d_{3j}^{(1)}|$ and $|e_{3j}^{(1)}|$ and with the moderate anisotropy of $d_{3j}^{(1)}$ and $e_{3j}^{(1)}$. The second composition is a "hard" modified $PbTiO_3$ FC (I) with a large anisotropy of $d_{3j}^{(1)}$ and $e_{3j}^{(1)}$ at $e_{3j}^{(1)} > 0$. A piezo-passive polymer component can be chosen, for example, among compositions listed in Table 3.1.

It is assumed that the 2–2 composite represents a system of parallel-connected FC and polymer layers, and these layers form a regular laminar structure (Fig. 3.2). In the initial state (at the orientation angle $\alpha = 0°$ or $\beta = 0°$, see insets 1 and 2 in Fig. 3.2), the remanent polarisation vector in each FC layer is $\boldsymbol{P}_r^{(1)} || OX_3$. Hereafter we consider rotations of the $\boldsymbol{P}_r^{(1)}$ vector around one of the co-ordinate axes, OX_1 or OX_2, as shown in insets 1 and 2 in Fig. 3.2, and the FC layers in the composite sample have the same appointed orientation of $\boldsymbol{P}_r^{(1)}$. Subscripts "(1)" and "(2)" refer to the FC and polymer component, respectively. As mentioned earlier, the electrodes at the composite sample are perpendicular to the OX_3 axis.

Table 3.1 Elastic compliances $s_{ab}^{(n)}$ (in10^{-12}Pa^{-1}) and dielectric permittivity $\varepsilon_{pp}^{(n)}$ of piezo-passive polymers at room temperature

Polymer	$s_{11}^{(n)}$	$s_{12}^{(n)}$	$\varepsilon_{pp}^{(n)}/\varepsilon_0$
Araldite [14]	216	−78	4.0
Polyurethane [15]	405	−151	3.5
Elastomer [16]	3,300	−1, 480	5.0

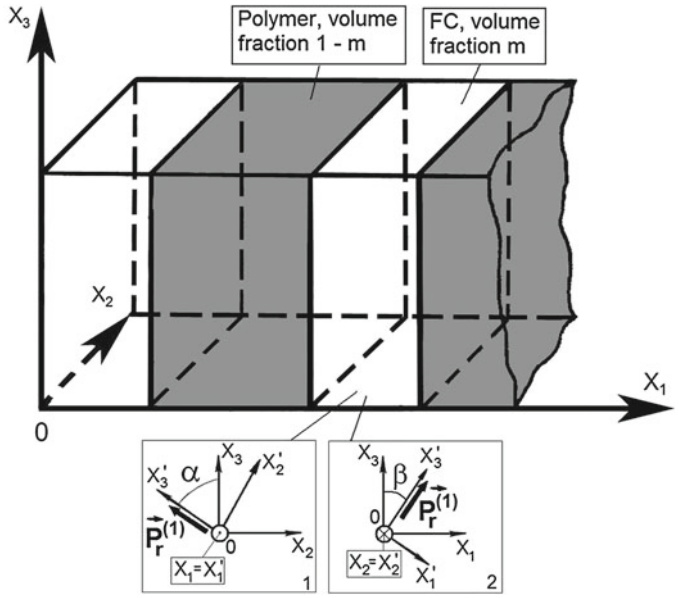

Fig. 3.2 Schematic of the 2–2 FC/polymer composite. $(X_1X_2X_3)$ is the rectangular co-ordinate system of the composite sample, α and β are angles of rotation of the remanent polarisation vector $\boldsymbol{P}_r^{(1)} || OX_3'$ of the FC layer around either the OX_1 axis (*inset 1*) or the OX_2 axis (*inset 2*)

The effective electromechanical properties of the composite studied are determined within the framework of the matrix approach [2] that is applied to piezoactive composite materials with planar microgeometry. The matrix of the effective properties of the composite in the co-ordinate system $(X_1X_2X_3)$

$$\| C^* \| = \begin{pmatrix} \| s^{*E} \| & \| d^* \|^t \\ \| d^* \| & \| \varepsilon^{*\sigma} \| \end{pmatrix} \tag{3.4}$$

is written in terms of $||s^{*E}||$ (6×6 matrix), $||d^*||$(3×6 matrix) and $||\varepsilon^{*\sigma}||$($3 \times 3$ matrix), and superscript "t" in (3.1) denotes the transposed matrix. The $||C^*||$ matrix from (3.4) is determined by averaging the electromechanical properties of the components on the volume fraction m and is given by

$$||C^*|| = [||C^{(1)}|| \cdot ||M||m + ||C^{(2)}||(1-m)] \cdot [||M||m + ||I||(1-m)]^{-1}, \tag{3.5}$$

where $||C^{(1)}||$ and $||C^{(2)}||$ are matrices of the electromechanical properties of the FC and polymer component, respectively, $||M||$ is concerned with the electric and mechanical boundary conditions [2] at interfaces $x_1 = \text{const}$ (Fig. 3.2), and $||I||$ is the identity 9×9 matrix. Elements of the $||C^{(1)}||$ matrix are written taking into account

the orientation of $\boldsymbol{P}_r{}^{(1)}$ in the FC layer [see Eq. (2.1)]. The boundary conditions at $x_1 = \text{const}$ (Fig. 3.2) imply a continuity of components of mechanical stress $\sigma_{11} = \sigma_1$, $\sigma_{12} = \sigma_6$ and $\sigma_{13} = \sigma_5$, strain $\xi_{22} = \xi_2$, $\xi_{23} = \xi_4/2$ and $\xi_{33} = \xi_3$, electric displacement D_1, and electric field E_2 and E_3. The $||M||$ matrix from (3.5) is written for $x_1 = \text{const}$ in the general form as $||M|| = ||m_1||^{-1}||m_2||$ where

$$\| m_n \| = \begin{pmatrix} 1 & 0 & 0 & 0 & 0 & 0 & 0 & 0 & 0 \\ s_{12}^{(n),E} & s_{22}^{(n),E} & s_{23}^{(n),E} & s_{24}^{(n),E} & s_{25}^{(n),E} & s_{26}^{(n),E} & d_{12}^{(n)} & d_{22}^{(n)} & d_{32}^{(n)} \\ s_{13}^{(n),E} & s_{23}^{(n),E} & s_{33}^{(n),E} & s_{34}^{(n),E} & s_{35}^{(n),E} & s_{36}^{(n),E} & d_{13}^{(n)} & d_{23}^{(n)} & d_{33}^{(n)} \\ s_{14}^{(n),E} & s_{24}^{(n),E} & s_{34}^{(n),E} & s_{44}^{(n),E} & s_{45}^{(n),E} & s_{46}^{(n),E} & d_{14}^{(n)} & d_{24}^{(n)} & d_{34}^{(n)} \\ 0 & 0 & 0 & 0 & 1 & 0 & 0 & 0 & 0 \\ 0 & 0 & 0 & 0 & 0 & 1 & 0 & 0 & 0 \\ d_{11}^{(n)} & d_{12}^{(n)} & d_{13}^{(n)} & d_{14}^{(n)} & d_{15}^{(n)} & d_{16}^{(n)} & \varepsilon_{11}^{(n),\sigma} & \varepsilon_{12}^{(n),\sigma} & \varepsilon_{13}^{(n),\sigma} \\ 0 & 0 & 0 & 0 & 0 & 0 & 0 & 1 & 0 \\ 0 & 0 & 0 & 0 & 0 & 0 & 0 & 0 & 1 \end{pmatrix}$$

is represented in terms of the electromechanical contants of the components ($n = 1$ or 2).

Rotation matrices related to the orientations of $\boldsymbol{P}_r^{(1)}$ (see insets 1 and 2 in Fig. 3.2) are given by

$$\| r(\alpha) \| = \begin{pmatrix} 1 & 0 & 0 \\ 0 & \cos\alpha & \sin\alpha \\ 0 & -\sin\alpha & \cos\alpha \end{pmatrix} \tag{3.6}$$

and

$$\| r(\beta) \| = \begin{pmatrix} \cos\beta & 0 & -\sin\beta \\ 0 & 1 & 0 \\ \sin\beta & 0 & \cos\beta \end{pmatrix}, \tag{3.7}$$

respectively. Thus, elements of $||C^*||$ from (3.2) depend either on m and α (rotation mode in inset 1 in Fig. 3.2) or on m and β (rotation mode in inset 2 in Fig. 3.2). We do not consider the case of a rotation of $\boldsymbol{P}_r{}^{(1)}$ around the OX_3 axis while the

piezoelectric coefficients of the FC component poled along OX_3 [9] obey an equality $d_{31}^{(1)} = d_{32}^{(1)}$.

Taking into account the $||d||$ matrix related to the FC component poled along the OX_3 axis (∞mm symmetry, see Sect. 1.1), Eq. (2.1) and rotation matrices from (3.6) and (3.7), we find the $||d||$ matrix at various angles α and β. At $0° < \alpha < 90°$ the $||d||$ matrix is written as

$$\| d \| = \begin{pmatrix} 0 & 0 & 0 & 0 & d_{15} & d_{16} \\ d_{21} & d_{22} & d_{23} & d_{24} & 0 & 0 \\ d_{31} & d_{32} & d_{33} & d_{34} & 0 & 0 \end{pmatrix},$$

however for $\alpha = 90°$ we have

$$\| d \| = \begin{pmatrix} 0 & 0 & 0 & 0 & 0 & d_{16} \\ d_{21} & d_{22} & d_{21} & 0 & 0 & 0 \\ 0 & 0 & 0 & d_{16} & 0 & 0 \end{pmatrix}.$$

We also examine that

$$\| d \| = \begin{pmatrix} d_{11} & d_{12} & d_{13} & 0 & d_{15} & 0 \\ 0 & 0 & 0 & d_{24} & 0 & d_{26} \\ d_{31} & d_{32} & d_{33} & 0 & d_{35} & 0 \end{pmatrix}$$

at $0° < \beta < 90°$ and

$$\| d \| = \begin{pmatrix} d_{11} & d_{12} & d_{12} & 0 & 0 & 0 \\ 0 & 0 & 0 & 0 & 0 & d_{26} \\ 0 & 0 & 0 & 0 & d_{26} & 0 \end{pmatrix}$$

at $\beta = 90°$ take place. The $||e||$ matrix has the form similar to that of $||d||$. Certainly, the orientation of the poled FC component influences the piezoelectric performance and anisotropy of the composite shown in Fig. 3.2.

To characterise the piezoelectric anisotropy of the studied 2–2 composite at $\alpha \neq 90°$ and $\beta \neq 90°$, we introduce anisotropy factors as follows:

$$\zeta_{d31} = d_{33}^*/d_{31}^* \text{ and } \zeta_{d32} = d_{33}^*/d_{32}^* \tag{3.8}$$

(for d^*_{3j} and $g^*_{3j} = d^*_{3j}/\varepsilon^{*\sigma}_{33}$), and

$$\zeta_{e31} = e^*_{33}/e^*_{31} \text{ and } \zeta_{e32} = e^*_{33}/e^*_{32} \tag{3.9}$$

(for e^*_{3j} and $h^*_{3j} = e^*_{3j}/\varepsilon^{*\xi}_{33}$). Equations (3.8) for the converse piezoelectric effect are represented as ratios of piezoelectric strains ξ_{33}/ξ_{11} and ξ_{33}/ξ_{22} as a result of the electric field $\boldsymbol{E_3}||OX_3$ in accordance with (1.6). Equations (3.9) enable us to evaluate ratios of piezoelectric polarisations, and therefore, ratios of surface charge densities, caused by external strains ξ_{jj} at the direct piezoelectric effect. According to (1.5), the piezoelectric polarisation P^*_3 of the composite (Fig. 3.2) equals $e^*_{33}\xi_3$ in the field of the longitudinal strain ξ_3, $e^*_{32}\xi_2$ in the field of the transverse strain ξ_2 or $e^*_{31}\xi_1$ in the field of the transverse strain ξ_1.

The anisotropy factors (3.8) and (3.9) are of value for high-anisotropic piezoactive elements that are used, for instance, in medical diagnostic devices with ultrasonic antennae based on pulse-echo principles and control of the preferred direction, in hydrophones, and other acoustic devices [17]. It should be added that various applications for high-anisotropic elements are attempting to effectively remove the interaction between the thickness and lateral vibration modes in the vicinity of the resonance of the thickness mode [17].

Examples of the volume-fraction and orientation behaviour of the anisotropy factors (3.8) and (3.9) are shown in Figs. 3.3 and 3.4. Graphs of the longitudinal piezoelectric coefficients e^*_{33} and d^*_{33} are represented in Fig. 3.5. Distinctions between the graphs in Figs. 3.3 and 3.4 are accounted for by the role of the elastic and piezoelectric properties in forming the piezoelectric anisotropy of the 2–2 composite. It is seen that the anisotropy factors ζ_{e3j} undergo considerably more changes than ζ_{d3j} irrespective of the FC component (cf. Figs. 3.3 and 3.4). Moreover, the longitudinal piezoelectric response concerned with e^*_{33} and d^*_{33} is similar, i.e., the anisotropy of the electromechanical properties of the FC component does not influence the configuration of curves in Fig. 3.5. The drastic changes in ζ_{e3j} may be a result of the presence of a system of interfaces $x_1 = \text{const}$ (Fig. 3.2) and the effect of the orientation of $\boldsymbol{P}_r{}^{(1)}$ of the FC on their elastic and piezoelectric properties and the effective properties of the composite as a whole. Taking into account the orientation effect and Eq. (1.12), one can write the anisotropy factors (3.8) in the general form as follows:

$$\zeta_{d31} = e^*_{3q}s^{*E}_{q3}/(e^*_{3q}s^{*E}_{q1}) = (e^*_{31}s^{*E}_{13} + e^*_{32}s^{*E}_{23} + \ldots + e^*_{36}s^{*E}_{63})/(e^*_{31}s^{*E}_{11} + e^*_{32}s^{*E}_{21} + \ldots + e^*_{36}s^{*E}_{61}) \text{ and } \zeta_{d32} = e^*_{3q}s^{*E}_{q3}/(e^*_{3q}s^{*E}_{q2}) = (e^*_{31}s^{*E}_{13} + e^*_{32}s^{*E}_{23} + \ldots + e^*_{36}s^{*E}_{63})/(e^*_{31}s^{*E}_{12} + e^*_{32}s^{*E}_{22} + \ldots + e^*_{36}s^{*E}_{62}). \tag{3.10}$$

The presence of the $e^*_{3q}\ s^{*E}_{q3}$-type terms in (3.10) leads to a simultaneous influence of the anisotropy of both e^*_{3j} and s^{*E}_{ab} on the anisotropy of d^*_{3j}, and we observe smooth

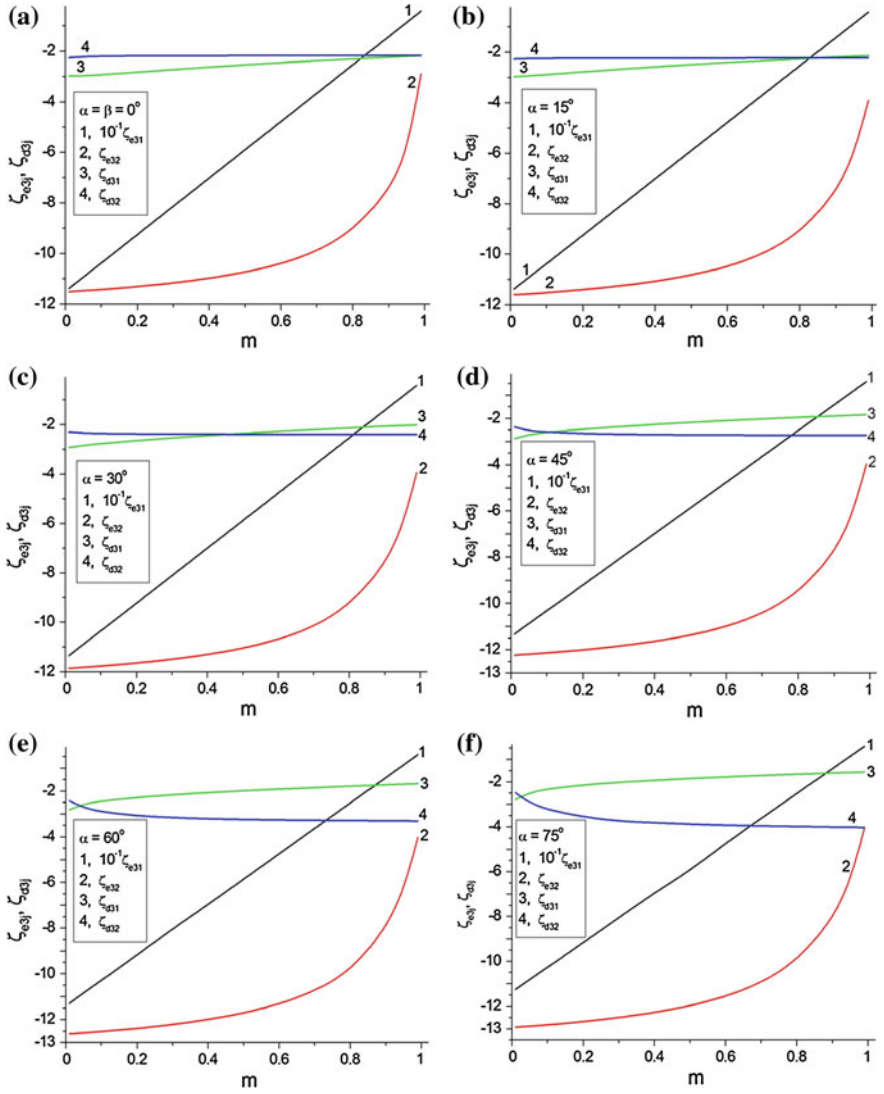

Fig. 3.3 Volume-fraction dependences of the anisotropy factors ζ_{e3j} and ζ_{d3j} of the 2–2 PCR-7M FC/polyurethane composite at $\alpha = \beta = 0°$ (**a**), $\alpha = \text{const} > 0°$ (**b–f**) and $\beta = \text{const} > 0°$ (**g–k**). Modes of rotation of the remanent polarisation vector $\boldsymbol{P}_r^{(1)}$ are shown in *insets* 1 and 2 in Fig. 3.2

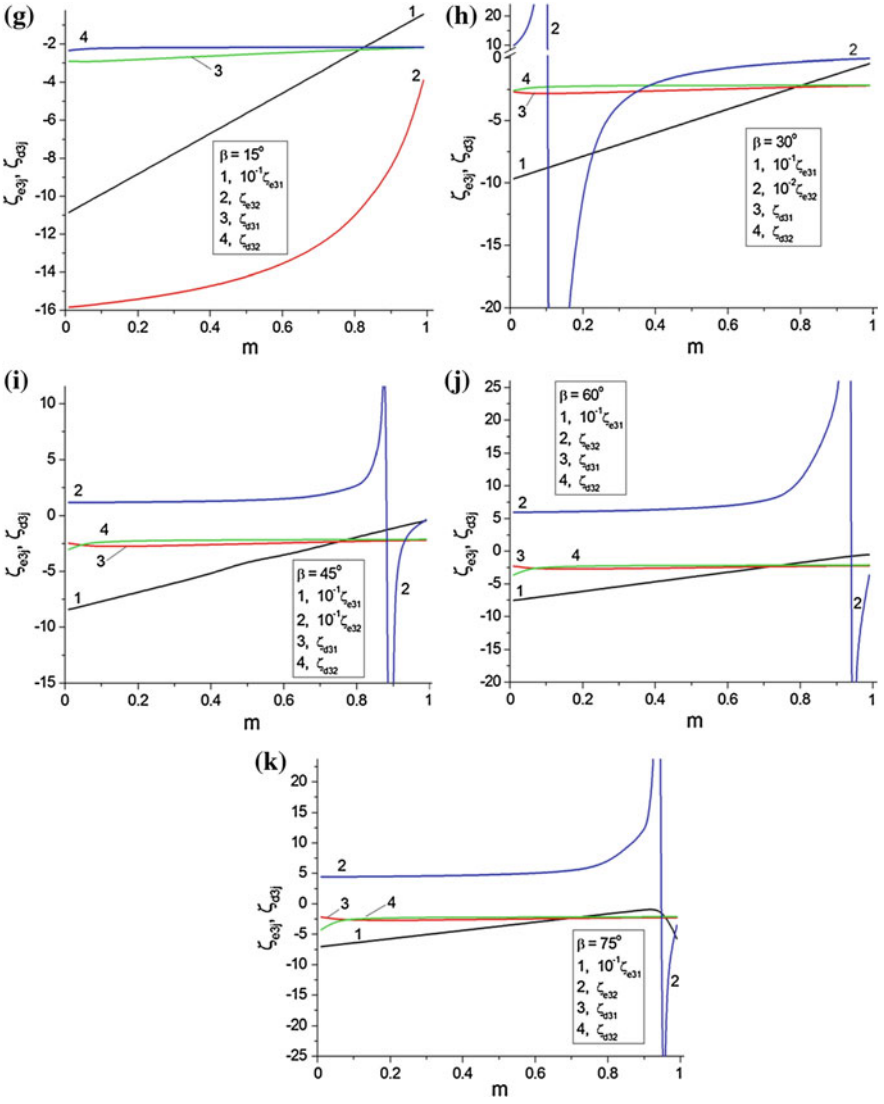

Fig. 3.3 (continued)

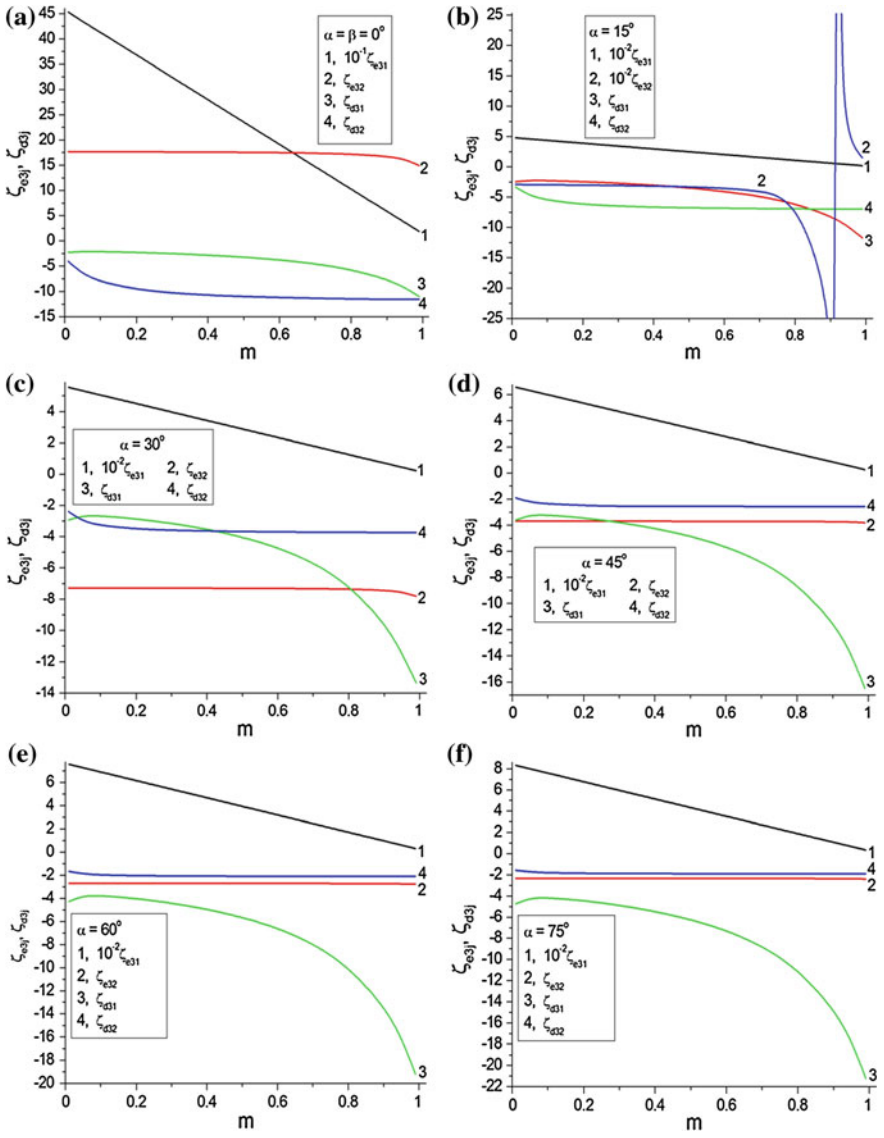

Fig. 3.4 Volume-fraction dependences of anisotropy factors ζ_{e3j} and ζ_{d3j} of the 2–2 modified $PbTiO_3$ FC/polyurethane composite at $\alpha = \beta = 0°$ (**a**), $\alpha = \text{const} > 0°$ (**b–f**) and $\beta = \text{const} > 0°$ (**g–k**). Modes of rotation of the remanent polarisation vector $\boldsymbol{P}_r^{(1)}$ are shown in insets 1 and 2 in Fig. 3.2

curves of ζ_{d3j} that change in restricted ranges (Figs. 3.3 and 3.4). It is also noteworthy that the anisotropy factors (3.9) obey conditions $\zeta_{e3j} \to \pm\infty$ (Figs. 3.3 and 3.4) in specific ranges of angles α and β. We see that the condition

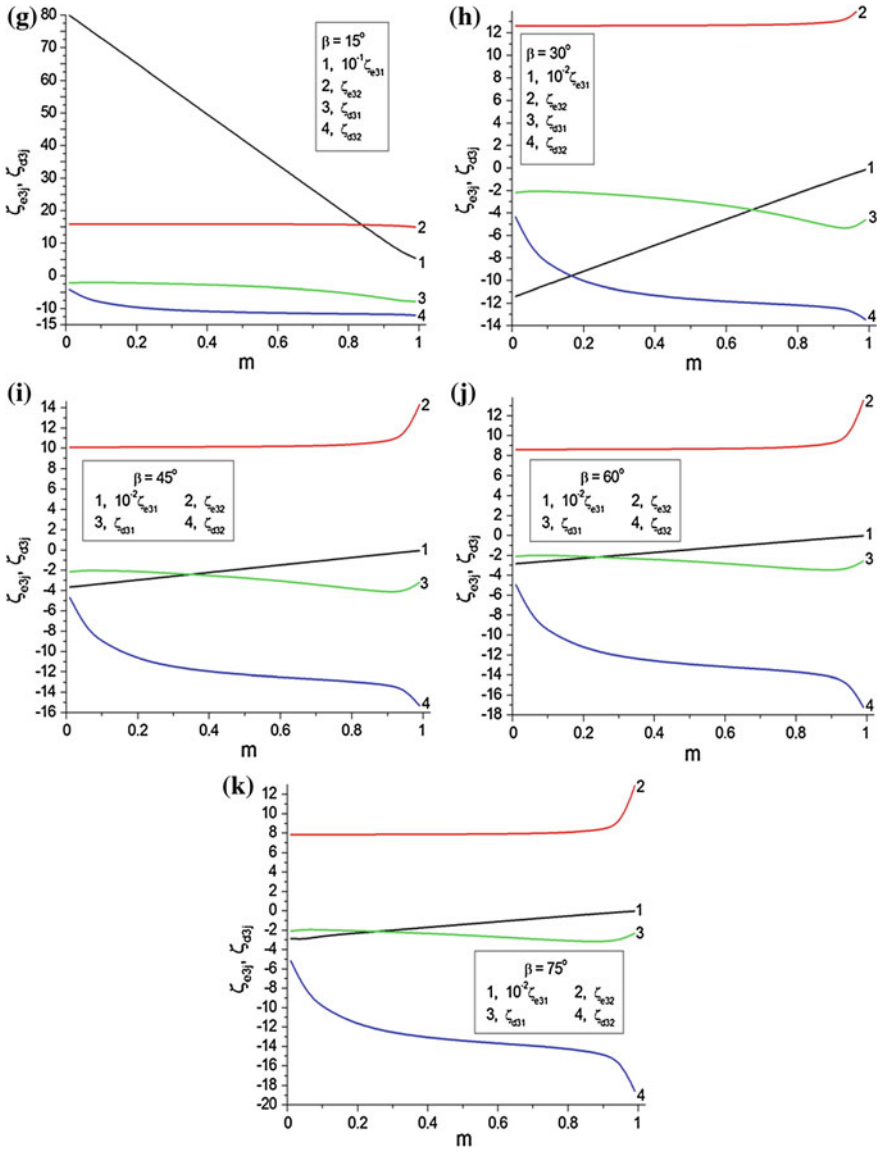

Fig. 3.4 (continued)

$$\zeta_{e32} \rightarrow \pm\infty \tag{3.11}$$

is achieved in the composite based on the modified $PbTiO_3$ FC (Fig. 3.4b), and this FC component is characterised by piezoelectric coefficients $e_{3j}^{(1)} > 0$ and $e_{15}^{(1)} > 0$. Such behaviour may be a result of the variable elastic anisotropy of the composite

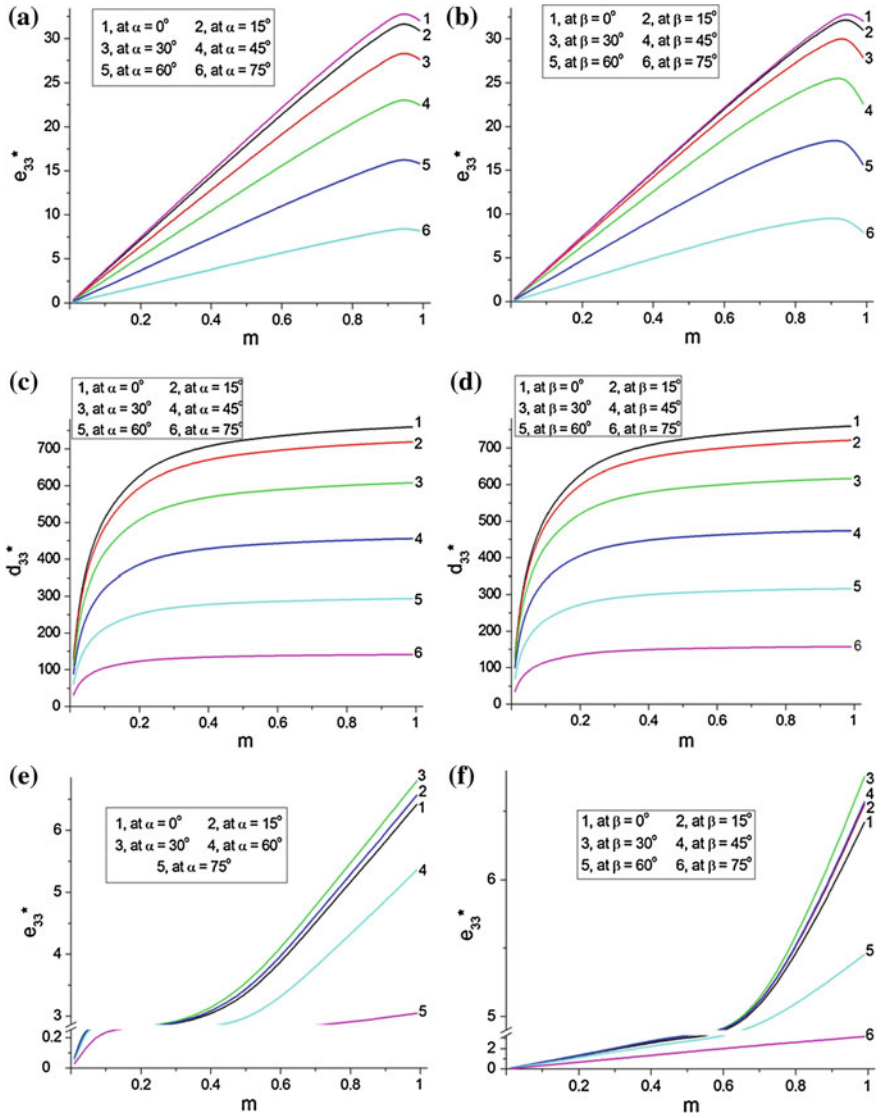

Fig. 3.5 Volume-fraction dependences of piezoelectric coefficients e_{33}^* (in C/m^2) and d_{33}^* (in pC/N) of the 2–2 PCR-7M FC/polyurethane composite (**a**–**d**) and a modified $PbTiO_3$ FC/polyurethane composite (**e**–**h**). Modes of rotation of the remanent polarisation vector $\boldsymbol{P}_r^{(1)}$ are shown in *insets* 1 and 2 in Fig.3.2

wherein the remanent polarisation vector $\boldsymbol{P}_r^{(1)}$ undergoes rotations in the plane of the interfaces (see inset 1 in Fig. 3.2). The same condition (3.11) is also valid in a relatively wide range of β in the composite based on the PCR-7M FC (Fig. 3.3h–k). In

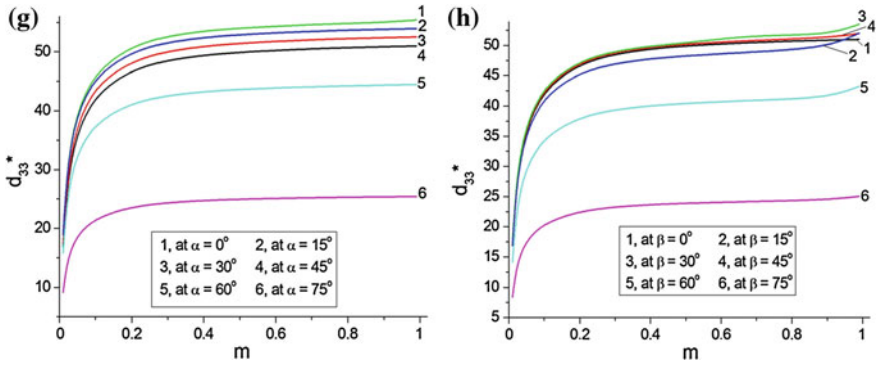

Fig. 3.5 (continued)

this composite the $\boldsymbol{P}_r^{(1)}$ vector undergoes rotations in the plane that is perpendicular to the interfaces (see inset 2 in Fig. 3.2), and the piezoelectric coefficients of the PCR-7M FC obey the condition [2]

$$\operatorname{sgn} e_{31}^{(1)} = -\operatorname{sgn} e_{33}^{(1)} = -\operatorname{sgn} e_{15}^{(1)} \tag{3.12}$$

In our opinion, such a rotation mode and the valid condition (3.12) favour the anisotropy of e_{3j}^* in the PCR-7M-based composite. In contrast to e_{3j}^*, the piezoelectric coefficients d_{3j}^* do not provide a large anisotropy at any variations of α and β (Fig. 3.3), and this performance may be due to the compensatory role of the aforementioned $e_{3q}^*\ s_{q3}^{*E}$-type terms in (3.10).

3.2 Single Crystal/Polymer Composites

3.2.1 Composites with Single-Domain Single-Crystal Components

3.2.1.1 PMN–*x*PT Single Crystals in 2–2 Composites

PMN–0.33PT has been the first perovskite-type relaxor-ferroelectric SC for which the full sets of the electromechanical constants were measured in both the single-domain and polydomain (domain-engineered) states at room temperature (see data in Tables 1.1 and 2.1). We highlight that the PMN–0.33PT SC is characterised by 3*m* or 4*mm* symmetry [18, 19] in the single-domain or polydomain state, respectively, and the molar concentration $x = 0.33$ indicates that this composition is located very close to the MPB [20]. In the single-domain state, the piezoelectric properties of the PMN–0.33PT SC have been analysed for various orientations of the main crystallographic axes [21], and some interconnections between the electromechanical

Table 3.2 Elastic compliances $s_{ab}^{(n),E}$ (in 10^{-12}Pa^{-1}), piezoelectric coefficients $d_{ij}^{(n)}$ (in pC/N) and dielectric permittivity $\varepsilon_{pp}^{(n),\sigma}$ of poled PMN–0.28PT SCs at room temperature [22]

Electromechanical constants	Single-domain $[111]_c$ -poled SC, $3m$ symmetry	Polydomain $[001]_c$ -poled SC, $4mm$ symmetry	Polydomain $[011]_c$-poled SC, $mm2$ symmetry
$s_{11}^{(n),E}$	8.78	44.57	13.40
$s_{12}^{(n),E}$	−4.90	−28.91	−21.18
$s_{13}^{(n),E}$	−0.93	−13.91	12.67
$s_{14}^{(n),E}$	16.87	0	0
$s_{22}^{(n),E}$	8.78	44.57	54.36
$s_{23}^{(n),E}$	−0.93	−13.91	−33.59
$s_{33}^{(n),E}$	6.32	34.38	28.02
$s_{44}^{(n),E}$	138.69	15.22	15.22
$s_{55}^{(n),E}$	138.69	15.22	147.06
$s_{66}^{(n),E}$	27.4	16.34	22.47
$d_{15}^{(n)}$	2,382	122	2,162
$d_{22}^{(n)}$	−312	0	0
$d_{24}^{(n)}$	2382	122	160
$d_{31}^{(n)}$	−43	−569	447
$d_{32}^{(n)}$	−43	−569	−1, 150
$d_{33}^{(n)}$	97	1,182	860
$\varepsilon_{11}^{(n),\sigma}/\ \varepsilon_0$	4,983	1,672	4,235
$\varepsilon_{22}^{(n),\sigma}/\ \varepsilon_0$	4,983	1,672	1,081
$\varepsilon_{33}^{(n),\sigma}/\ \varepsilon_0$	593	5,479	3,873

Data on the $[001]_c$- and $[011]_c$-poled polydomain SCs are related to their main crystallographic axes

properties of the single-domain and polydomain SCs were discussed in Chap. 2. To the best of our knowledge, PMN–0.28PT is the first relaxor-ferroelectric SC, for which self-consistent and full sets of electromechanical constants (Table 3.2) have been measured [22] along three poling directions, namely, along $[111]_c$, $[001]_c$ and $[011]_c$ in the perovskite unit cell. In the single-domain state at room temperature, the PMN–0.28PT SC is characterised by 3 m symmetry with a spontaneous polarisation vector $\boldsymbol{P}_s{}^{(1)} \parallel [111]_c$. The domain-engineered SC poled along $[001]_c$ exhibits $4mm$ symmetry and has an average spontaneous polarisation vector $\boldsymbol{P}_s{}^{(1)} \parallel [001]_c$. Poling along the $[011]_c$ axis leads to the domain-engineered state with $mm2$ symmetry and an average spontaneous polarisation vector $\boldsymbol{P}_s{}^{(1)} \parallel [011]_c$. As noted by Liu et al. [22], the full sets of electromechanical constants (Table 3.2) were determined from the same PMN–0.28PT crystal wafer, so that the composition and properties are uniform. Experimental data on PMN–xPT SCs (Tables 1.1, 2.1 and 3.2) enable a comparison of the effective electromechanical properties of the SC/polymer composites that comprise either the single-domain or polydomain SC component and are characterised by the same connectivity pattern.

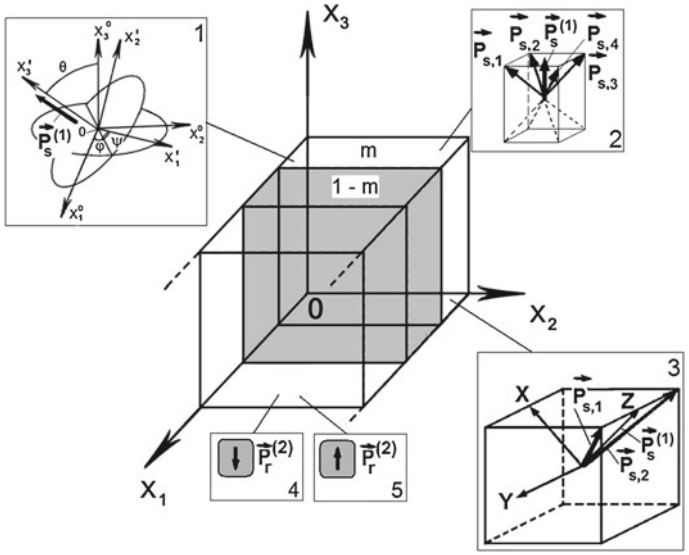

Fig. 3.6 Schematic of a 2–2 SC/polymer composite. ($X_1X_2X_3$) is the rectangular co-ordinate system, m and $1 - m$ are volume fractions of SC and polymer, respectively, $\boldsymbol{P}_s^{(1)}$ and $\boldsymbol{P}_r^{(2)}$ are the spontaneous polarisation vector of SC and the remanent polarisation vector of polymer, respectively. In *inset 1* φ, ψ and θ are Euler angles that characterise a rotation of the main crystallographic axes $(X_1^oX_2^oX_3^o) \rightarrow (X_1\prime X_2\prime X_3\prime)$ and the $\boldsymbol{P}_s^{(1)}$ vector in each single-domain SC layer. *Inset 2* comprises domain orientations in the $[001]_c$-poled SC with the effective spontaneous polarisation vector $\boldsymbol{P}_s^{(1)}$, *inset 3* comprises domain orientations in the $[011]_c$-poled SC with the effective spontaneous polarisation vector $\boldsymbol{P}_s^{(1)}$. $\boldsymbol{P}_{s,1}$, $\boldsymbol{P}_{s,2}$, $\boldsymbol{P}_{s,3}$, and $\boldsymbol{P}_{s,4}$ are spontaneous polarisation vectors of several domain types. x, y and z are the main crystallographic axes of the polydomain SC shown in *inset 3*. The remanent polarisation vector of polymer $\boldsymbol{P}_r^{(2)} \uparrow\downarrow OX_3$ can be oriented as shown in *insets 4* and *5*

The 2–2 SC/polymer composite (Fig. 3.6) is characterised by a regular distribution of alternating SC and polymer layers in the OX_1 direction, and the layers are assumed to be lengthy in the OX_2 and OX_3 directions. The layers of polyvinylidene fluoride ferroelectric polymer (PVDF, see data in Table 3.3) have a remanent polarisation vector oriented as shown in insets 4 and 5 in Fig. 3.6: either $\boldsymbol{P}_r^{(2)} \uparrow\downarrow OX_3$ (PVDF-1 in the composite sample) or $\boldsymbol{P}_r^{(2)} \uparrow\uparrow OX_3$ (PVDF-2 in the composite sample). The manufacture of 2–2 composites having components with various orientations of the $\boldsymbol{P}_s^{(1)}$ and $\boldsymbol{P}_r^{(2)}$ vectors can be achieved by individually poling the components. In respect of the studied SC/polymer composite, the coercive fields $E_c^{(n)}$ of the relaxor-ferroelectric SC ($n = 1$) and polymer ($n = 2$) obey an inequality [23, 24] $E_c^{(1)} << E_c^{(2)}$, that favours this type of the poling process. It is also assumed that the electrodes for the composite sample are perpendicular to the OX_3 axis (Fig. 3.6). A biased electric field can be also applied to the composite sample in order to maintain the single-domain state in the SC layers.

The procedure for averaging the electromechanical properties in the 2–2 SC/polymer composite is performed within the framework of the matrix method taking into consideration the boundary conditions for electric and mechanical fields in the adjacent layers of the composite sample (see Sect. 3.1).

3.2.1.2 2–2 Composite Based on PMN–0.33PT Single Crystal

Now we consider the effective piezoelectric coefficients $\Pi^*_{33}(m, \varphi, \psi, \theta)$ ($\Pi = d, e$ and g) of the PMN–0.33PT-based composite that contains PVDF-1 with the piezoelectric coefficients $d^{(2)}_{31} < 0, d^{(2)}_{33} > 0$ and $d^{(2)}_{15} > 0$. Such signs of the piezoelectric coefficients are typical of many perovskite-type FCs based on $BaTiO_3$, $Pb(Zr, Ti)O_3$ etc. (see Table 1.2). The piezoelectric coefficient d^*_{33} is directly determined from (3.5), while e^*_{33} and g^*_{33} are determined using Eqs. (1.12), (1.13) and (1.16). The orientation of the $\boldsymbol{P}^{(1)}_{\boldsymbol{s}}$ vector is characterised by a θ angle at $\varphi = \psi = 0°$ (see inset 1 in Fig. 3.6). It is worth noting, that even in the simplest case of the orientation of $\boldsymbol{P}^{(1)}_{\boldsymbol{s}}$, one can obtain a non-monotonic dependence of $\Pi^*_{33}(m, 0°, 0°, \theta)$ on θ (Fig. 3.7) or m (Fig. 3.7b, c). At volume fractions $m \to 1$ the polymer layers have a small influence on the piezoelectric performance of the composite. As a consequence, the orientation dependences of the piezoelectric coefficients d^*_{33} and e^*_{33} on m (Fig. 3.7a, b) are similar to those studied for the single-domain PMN–0.33PT SC (see Sect. 2.1). As observed in conventional 2–2 FC/polymer composites [2, 11], max $g^*_{33}(m, 0°, 0°, \theta)$ is observed at $m << 1$ and $\theta \leq 50°$(Fig. 3.7c).

Relatively small volume fractions of the SC component $0 < m < 0.1$ lead to a non-monotonic behaviour of g^*_{33} in the piezo-active composite [2] due to the effect of dielectric properties of polymer on piezoelectric sensitivity in accordance with (1.12) and (1.14). An increase in θ has a significant effect of the balance of the piezoelectric coefficients $d^{(1)}_{ij}$ and $g^{(1)}_{ij}$ of the single-domain PMN–0.33 PT SC, and these changes promote a non-monotonic behaviour of g^*_{33} at $m = \text{const}$ (Fig. 3.7c). We show the graph of $g^*_{33}(m, 0°, 0°, \theta)$ at volume fractions $0 \leq m \leq 0.2$ only (see Fig. 3.7c) due to the rapid decrease in $|g^*_{33}|$ at $m > 0.2$ and any θ values [26]. This decrease is caused by an intensive increase in dielectric permittivities $\varepsilon^{*\sigma}_{fh}$ of the composite in the same m range.

A presence of slight max $e^*_{33}(m, 0°, 0°, \theta)$ or min $e^*_{33}(m, 0°, 0°, \theta)$ at $0.9 < m < 1$ (Fig. 3.7b) is a result of the effect of elastic properties of the components on the piezoelectric response of the composite [see (1.13)] and with changes in the balance

Table 3.3 Elastic compliances $s^{(n),E}_{ab}$ (in 10^{-12} Pa^{-1}), piezoelectric coefficients $d^{(n)}_{ij}$ (in pC/N) and dielectric permittivity $\varepsilon^{(n),\sigma}_{pp}$ of poled PVDF at room temperature [25]

$s^{(n),E}_{11}$	$s^{(n),E}_{12}$	$s^{(n),E}_{13}$	$s^{(n),E}_{33}$	$s^{(n),E}_{44}$	$s^{(n)}_{66}$	$d^{(n)}_{15}$	$d^{(n)}_{31}$	$d^{(n)}_{33}$	$\frac{\varepsilon^{(n),\sigma}_{11}}{\varepsilon_0}$	$\frac{\varepsilon^{(n),\sigma}_{33}}{\varepsilon_0}$
333	−148	−87.5	299	1.90×10^4	943	38	−10.42	33.64	7.513	8.431

The orientation of the remanent polarisation vector is shown in inset 4 in Fig. 3.6

of the piezoelectric coefficients d_{ij}^* at relatively large volume fractions m. It should be mentioned that max e_{33}^* is also observed in the 2–2 FC/polymer composites (Fig. 3.5a, b) at various orientations of the remanent polarisation vector $\boldsymbol{P}_{\boldsymbol{r}}^{(1)}$ and sgn $e_{ij}^{(1)}$ in accordance with (3.12).

A comparison of graphs of $d_{33}^*(m, 0°, 0°, \theta)$, $e_{33}^*(m, 0°, 0°, \theta)$ and $g_{33}^*(m, 0°, 0°, \theta)$ (Fig. 3.7) enables us to discuss the effect of the combination of properties (in terms of work [2, 26, 27]) in the studied composite. As follows from (1.13) and (1.14), the piezoelectric coefficients e_{ij}^* are regarded as a combination of the piezoelectric and elastic properties, while the piezoelectric coefficients g_{ij}^* can be regarded as a combination of the piezoelectric and dielectric properties. When changing the θ angle, the elastic compliances $s_{ab}^{(1),E}$ of the single-domain PMN–0.33 PT SC vary to a

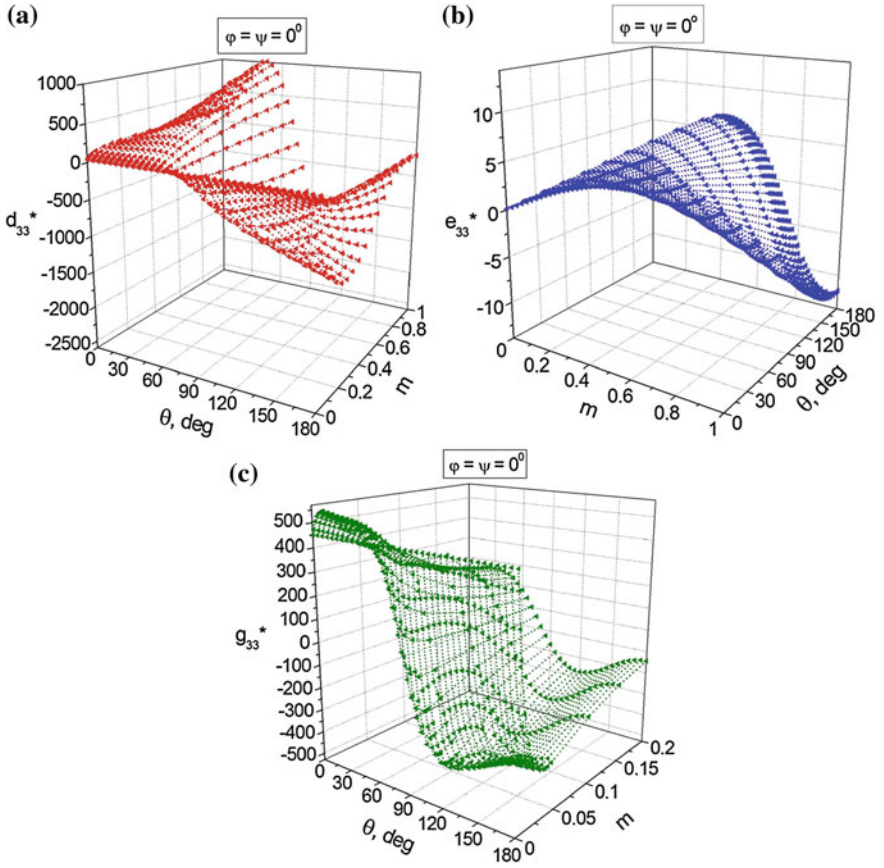

Fig. 3.7 Piezoelectric coefficients calculated for a 2–2 single-domain PMN–0.33PT SC/PVDF-1 composite: d_{33}^* (**a**, in pC/N), e_{33}^* (**b**, in C/m^2) and g_{33}^* (**c**, in mV·m/N) (reprinted from paper by Topolov and Krivoruchko [26], with permission from IOP Publishing)

lesser degree than the piezoelectric coefficients $d_{ij}^{(1)}$. We therefore see that the piezoelectric coefficient $e_{33}^*(m, 0°, 0°, \theta)$ varies in a fairly narrow range (Fig. 3.7b) owing to the dominating role of the elastic properties in forming this piezoelectric response. In contrast to $e_{33}^*(m, 0°, 0°, \theta)$, the piezoelectric coefficient $g_{33}^*(m, 0°, 0°, \theta)$ undergoes larger changes in the wide range (Fig. 3.7c), due to the considerable variations of both d_{ij}^* and $\varepsilon_{fh}^{*\sigma}$ in this composite.

3.2.1.3 Hydrostatic Parameters of the 2–2 Composite Based on PMN–xPT Single Crystal ($x = 0.28$ or 0.33)

In this section we compare the hydrostatic piezoelectric performance of 2–2 composites based on the single-domain PMN–xPT SCs. A prediction of the hydrostatic parameters and their extreme values is of importance for materials selection for hydroacoustic and other piezo-technical applications. Among these parameters, we study the hydrostatic piezoelectric coefficients d_h^* and g_h^* from (3.2), the hydrostatic piezoelectric coefficient

$$e_h^* = e_{33}^* + e_{32}^* + e_{31}^*, \tag{3.13}$$

the squared hydrostatic figure of merit $(Q_h^*)^2$ from (3.3), and the hydrostatic ECF

$$k_h^* = d_h^* / \sqrt{s_h^{*E} \varepsilon_{33}^{*\sigma}} \tag{3.14}$$

[see also (1.27)], where the hydrostatic compliance is given by $s_h^{*E} = \sum_{a=1}^{3} \sum_{b=1}^{3} s_{ab}^{*E}$ [15, 28]. The hydrostatic piezoelectric coefficients from (3.2) and (3.13) provide a measure of the activity and sensitivity of the composite under hydrostatic loading. $(Q_h^*)^2$ from (3.3) is introduced to evaluate the sensor signal-to-noise ratio of the composite and to characterise its piezoelectric sensitivity [2, 11, 16]. The ECF k_h^* from (3.14) enables one to characterise the transducer efficiency of the composite under hydrostatic loading. We add that the hydrostatic parameters Π_h^* from (3.2), (3.3), (3.13) and (3.14) are related to the composite sample (Fig. 3.6) with electrodes that are perpendicular to the OX_3 axis, and therefore, the piezoelectric coefficients with subscripts 31, 32 and 33 are taken into consideration.

Data on absolute maxima of the hydrostatic parameters Π_h^* are represented in Table 3.4. Based on these data and comparing them, it is possible to conclude that the PMN–0.28PT-based composite is of interest as a material with the largest hydrostatic piezoelectric coefficient e_h^*, and the PMN–0.33PT-based composite is of value as a piezo-active material with the large absolute values of the hydrostatic parameters, d_h^*, g_h^*, $(Q_h^*)^2$, and k_h^*. This good performance is due not only to the ansiotropy of the piezoelectric coefficients $d_{ij}^{(1)}$ etc. in the single-domain state, but also to the

Table 3.4 Absolute maxima (minima) of hydrostatic parameters $\Pi_h^*(m, \varphi, \psi, \theta)$ of the 2–2 single-domain PMN–xPT SC/PVDF-1 composite

Π_h^*	$x = 0.28$		$x = 0.33$	
	Value of absolute maxΠ_h^*	m, φ, ψ, and θ which correspond to the value of maxΠ_h^*	Value of absolute maxΠ_h^* (or absolute min Π_h^*)	m, φ, ψ, and θ which correspond to the value of maxΠ_h^* (or min Π_h^*)
d_h^*	133 pC/N	$m = 0.238$, $\varphi = 0°$, $\psi = 0°$, and $\theta = 74°$	–322 pC/N[a]	$m = 0.311$, $\varphi = 0°$, $\psi = 0°$, and $\theta = 86°$
g_h^*	242 mV· m/N	$m = 0.007$, $\varphi = 60°$, $\psi = 90°$, and $\theta = 57°$	–252 mV· m/N[a]	$m = 0.029$, $\varphi = 60°$, $\psi = 90°$, and $\theta = 127°$
e_h^*	45.1 C/m^2	$m = 0.868$, $\varphi = 60°$, $\psi = 90°$, and $\theta = 76°$	–22.3 C/m^{2a}	$m = 0.831$, $\varphi = 60°$, $\psi = 90°$, and $\theta = 117°$
$(Q_h^*)^2$	$12.3 \cdot 10^{-12}$ Pa^{-1}	$m = 0.021$,$\varphi = 60°$, $\psi = 90°$, and $\theta = 63°$	$21.5 \cdot 10^{-12}$ Pa^{-1}	$m = 0.067$, $\varphi = 60°$, $\psi = 90°$, and $\theta = 123°$
k_h^*	0.217	$m = 0.027$, $\varphi = 60°$, $\psi = 90°$, and $\theta = 63°$	0.294	$m = 0.085$,$\varphi = 60°$, $\psi = 90°$, and $\theta = 124°$

[a] Absolute minimum value

anisotropy of the electromechanical properties of the composite due to its laminar structure (Fig. 3.6).

Values of $e_h^* \approx$ (40–45) C/m^2 (Fig. 3.8) can be achieved in PMN–0.28PT-based composites near the absolute maximum point even with deviations of the Euler angles of approximately 5–10°, and deviations of the volume fraction of about 0.1 are also possible. It is noted for comparison that the single-domain $[111]_c$-poled PMN–0.28PT SC is characterised [22] by $e_h^{(1)} = -2.93$ C/m^2 at $\varphi = \psi = \theta = 0°$ and by $e_h^{(1)} = -0.708$ C/m^2 at $\varphi = 60°$,$\psi = 90°$ and $\theta = 76°$ (these Euler angles are related to absolute max e_h^*, see Table 3.4). The significant elastic anisotropy of the single-domain PMN–0.28PT SC (see elastic compliances $s_{ab}^{(n),E}$ in the second column of Table 3.2) leads to an effective re-distribution of mechanical fields in the composite sample and a favourable balance of the contributions from the piezoelectric coefficients e_{3j}^* (Fig. 3.8) into e_h^* [see (3.13)]. Data from Table 3.4 and Fig. 3.8 suggest that the Euler angle θ plays a key role in achieving the large hydrostatic piezoelectric coefficient e_h^* of this composite, and this circumstance is due to the orientation of the spontaneous polarisation vector $\boldsymbol{P}_s^{(1)}$ in the single-domain SC layer (see inset 1 in Fig. 3.6). The Euler angles $\varphi = 60°$ and $\psi = 90°$ are of interest to achieve absolute maxima of the four hydrostatic parameters (Table 3.4). Such orientations of the main crystallographic axes of the $[111]_c$-poled SC lead to an obvious simplification of the matrix of the piezoelectric properties of the composite $||p^*||$ where $p = d$, e and g. At $0 < m \leq 1$, $\varphi = 60°$, $\psi = 90°$, and various values of θ, this matrix is represented as

$$||p^*|| = \begin{pmatrix} p_{11}^* & p_{12}^* & p_{13}^* & 0 & p_{15}^* & 0 \\ 0 & 0 & 0 & p_{24}^* & 0 & p_{26}^* \\ p_{31}^* & p_{32}^* & p_{33}^* & 0 & p_{35}^* & 0 \end{pmatrix}, \tag{3.15}$$

and elements p_{31}^*, p_{32}^* and p_{33}^* from (3.15) promote large hydrostatic parameters of the composite. The large values of e_h^* (Table 3.4) are achieved at the most simple orientation of the electrodes, i.e., perprendicular to the OX_3 axis (Fig. 3.6). In comparison to this result, the absolute max $e_h^* = 42.6$ C/m^2 and absolute min $e_h^* = -44.4$ C/m^2 were predicted for the hydrostatic piezoelectric coefficient $e_h^* = e_{11}^* + e_{12}^* + e_{13}^* + e_{21}^* + e_{22}^* + e_{23}^* + e_{31}^* + e_{32}^* + e_{33}^*$ in a similar 2–2 PMN–0.33PT single-domain SC/PVDF-1 composite [26], but with electrodes having a more complex geometry, namely, a system of parallel-connected conducting layers oriented along the X_1OX_2, X_1OX_3 and X_2OX_3 planes. We note that the absolute max $e_h^* = 45.1$ C/m^2 (Table 3.4) evaluated in accordance with (3.13) is approximately 3–5 times larger than the hydrostatic piezoelectric coefficient e_h of the well-known PZT-type FCs [2, 28].

As for the PMN–0.33PT-based composite, its hydrostatic performance has some advantages over PMN–0.28PT-based composites due to large absolute values of min Π_h^* (Table 3.4). A reason for these values is concerned with the balance of the

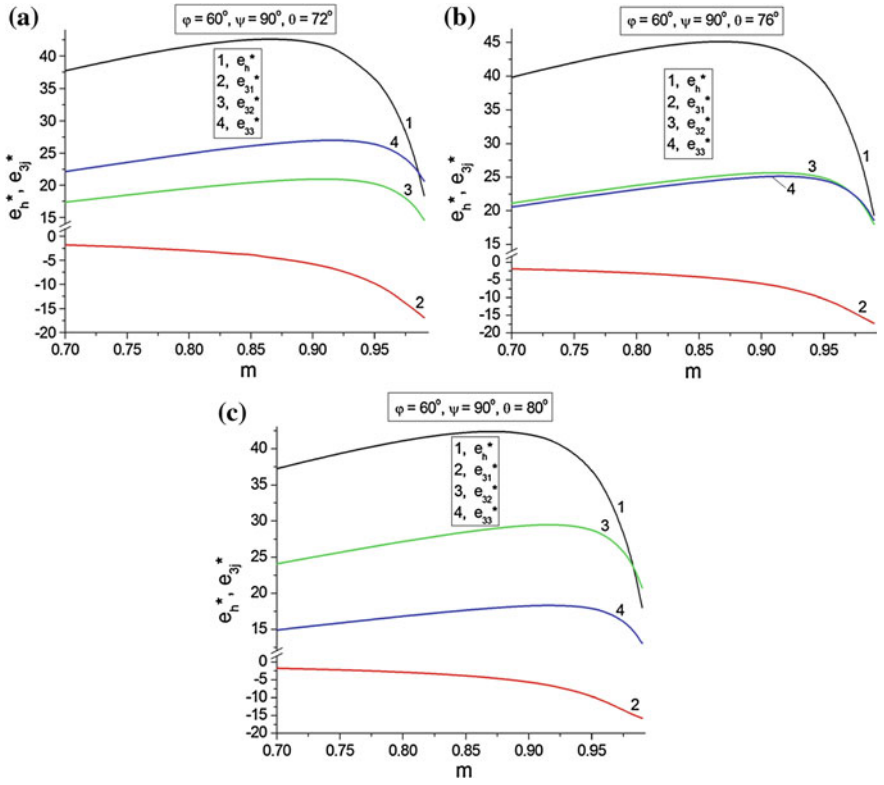

Fig. 3.8 Volume-fraction dependences of the piezoelectric coefficients e^*_{3j} and e^*_h (in $\mathrm{C/m^2}$) near absolute max $e^*_h(m, \varphi, \psi, \theta)$ in a 2–2 single-domain PMN–0.28PT SC/PVDF-1 composite at $\varphi = 60°, \psi = 90°$ and $\theta = 72°$ (**a**), $\varphi = 60°, \psi = 90°$ and $\theta = 76°$ (**b**), and $\varphi = 60°, \psi = 90°$ and $\theta = 80°$ (**c**)

piezoelectric coefficients $d^{(1)}_{ij}$ and with the anisotropy of elastic compliances $s^{(1),E}_{ab}$ of the single-domain PMN–0.33PT SC (see Table 2.1). A simple comparison of electromechanical constants from Tables 2.1 and 3.2 suggest that the single-domain PMN–0.33PT SC can be of value due to large positive values of both $d^{(1)}_{15}$ and $d^{(1)}_{22}$. The single-domain PMN–0.33PT SC is characterised by the large ratio $s^{(1),E}_{11}/s^{(1),E}_{33}$ (Table 2.1) that strongly influences the piezoelectric effect and its anisotropy in the composite. The absolute value of the hydrostatic piezoelectric coefficient $d^{(1)}_h$ of the single-domain PMN–0.33PT SC is also larger than that related to the single-domain PMN–0.28PT SC.

Thus, single-domain PMN–*x*PT SCs can be used to manufacture novel 2–2 composite with predictable hydrostatic parameters (Table 3.4). Criteria of the choice of the optimum SC component to achieve the largest $|\Pi^*_h|$ value may be formulated

in the future, after careful passing the molar-concentration range near the MPB and refining the full sets of electromechanical constants of SCs with related compositions.

3.2.2 Composites with Polydomain Single-Crystal Components: A Comparison of Hydrostatic Parameters

3.2.2.1 Composites Based on PMN–0.28PT Single Crystals

The next important step in the study of 2–2 SC/polymer composites is a comparison of the hydrostatic parameters that are achieved in the presence of a polydomain (domain-engineered) SC component with a specific domain arrangement. In Sect. 3.2.2 we will distinguish the following 2–2 composites:

(i) with polydomain $[001]_c$-poled SC layers (inset 2 in Fig. 3.6) and
(ii) with polydomain $[011]_c$-poled SC layers (inset 3 in Fig. 3.6).

We rotate the main crystallographic axes x, y and z of the polydomain SC layer in these composites around one of the co-ordinate axes–$OX_1||x$, $OX_2||y$ or $OX_3||$ z (see examples in Fig. 3.9). Such modes of rotation make it possible to maintain the polydomain state (insets 2 and 3 in Fig. 3.6) in the SC layer. It is assumed that at these rotations, the spontaneous polarisation vectors of domains $\boldsymbol{P_{s,1}}, \boldsymbol{P_{s,2}}$ etc. in the SC layer are situated either over or in the (X_1OX_2) plane (see Fig. 3.6). The rotation angles are varied in the following ranges [29–31]:

(i) for composites with $[001]_c$-poled layers, $-45° \leq \delta_x \leq 45°$ or $-45° \leq \delta_y \leq 45°$ (Fig. 3.9a), and
(ii) for composites with $[011]_c$-poled layers, $-\arcsin(1/\sqrt{3}) \leq \alpha \leq \arcsin(1/\sqrt{3})$, $-45° \leq \beta \leq 45°$ or $0° \leq \gamma \leq 360°$ (see Fig. 3.9b and inset 3 in Fig. 3.6).

Because of the 4*mm* symmetry of the $[001]_c$-poled PMN–0.28PT SC (see inset 2 in Fig. 3.6 and Table 3.2) and the equality of its piezoelectric coefficients $d_{31}^{(1)} = d_{32}^{(1)}$, we do not consider the mode of rotation of the main crystallographic axes x and y of this SC around $OX_3||$ z.

Values of absolute maxima of d_h^*, g_h^*, $(Q_h^*)^2$, and k_h^* of the composite with the $[001]_c$-poled layers are larger than those related to the composite with single-domain $[111]_c$-poled layers (cf. data in Tables 3.5 and 3.4). This is a result of the relatively high piezoelectric activity and the relatively small elastic anisotropy of the $[001]_c$-poled SC (see Table 3.2). As in the composite with single-domain $[111]_c$-poled layers, the absolute $\max g_h^*$ in the composite with $[001]_c$-poled layers is achieved at very low volume fraction of SC ($m < 1\,\%$), which could be problematic in terms of the manufacturing tolerance. The presence of $\max g_h^*$ at the small volume fractions m is due to the role of the dielectric properties of the polymer component [2, 26, 30, 31]: as is known, extreme points of piezoelectric coefficients g_{3j}^* in various two-component composites are observed in a volume-fraction range where the dielectric permittivity of the composite $\varepsilon_{33}^{*\sigma}$ obeys the condition $\varepsilon_{33}^{*\sigma} << \varepsilon_{33}^{(1),\sigma}$.

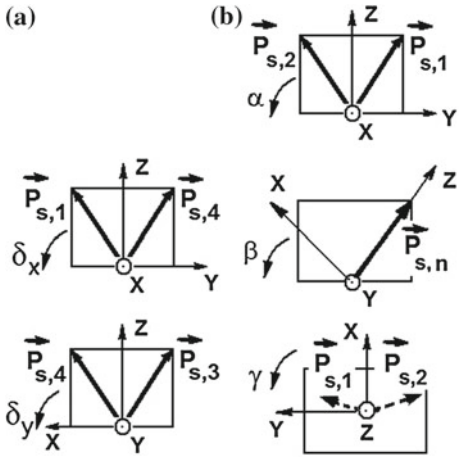

Fig. 3.9 Modes of rotation of the spontaneous polarisation vectors $\boldsymbol{P_{s,1}}$, $\boldsymbol{P_{s,2}}$, ... in the $[001]_c$-poled (**a**) and $[011]_c$-poled (**b**) SCs. x, y and z are the main crystallographic axes of the polydomain SC, δ_x and δ_y are rotation angles for the $[001]_c$-poled SC, and α, β and γ are rotation angles for the $[011]_c$-poled SC (reprinted from paper by Topolov et al. [29], with permission from Taylor and Francis)

The absolute maxima of d_h^*, g_h^*, $(Q_h^*)^2$, and k_h^* of the composite with $[011]_c$-poled layers (Table 3.5) are larger than those of the composites with single-domain (Table 3.4) and $[001]_c$-poled layers (Table 3.5). In our opinion, the high performance of the composite with $[011]_c$-poled layers is due to the unusual anisotropy of the electromechanical properties of the SC. For instance, in the $[011]_c$-poled PMN–0.28SC the elastic compliances $s_{ab}^{(n),E}$ are linked by the ratios

$$s_{11}^{(1),E} \approx s_{13}^{(1),E},\ |s_{23}^{(1),E}| \approx 2.7 s_{13}^{(1),E} \text{ and } s_{33}^{(1),E} \approx 2 s_{13}^{(1),E}, \tag{3.16}$$

while the piezoelectric coefficients $d_{3j}^{(n)}$ of the same SC obey the conditions

$$d_{33}^{(1)} \approx 1.9\, d_{31}^{(1)} \text{ and } |d_{32}^{(1)}| \approx 2.6\, d_{31}^{(1)} \tag{3.17}$$

(see Table 3.2). Variations of the rotation angles α and β lead to values of $\max \Pi_h^*$ which are lower than those in Table 3.5 for the composite with $[011]_c$-poled SC layers, and we omit results on $\Pi_h^*(m,\alpha)$ and $\Pi_h^*(m,\beta)$ for this composite.

The important advantage of composites with $[011]_c$-poled SC layers over the similar composites based on PMN–0.28PT is the optimal orientation of the main crystallographic axes of the $[011]_c$-poled state. In this case the five hydrostatic parameters $\Pi_h^*(m,\gamma)$ have absolute maxima at $\gamma = 90°$ and volume factions m from 0.012 to 0.876 (Table 3.5). It is worth noting that at $0 < m \leq 1$ and $\gamma = 90°$, the matrix $||d^*||$ of the piezoelectric coefficients of the composite with the $[011]_c$-poled SC layers has a form

Table 3.5 Absolute maxima of hydrostatic parameters Π_h^* of 2-2 polydomain PMN-0.28PT/ PVDF-1 composites

	Composite with $[001]_c$**-poled SC layers**		**Composite with** $[011]_c$**-poled SC layers**	
Π_h^*	Value of absolute maxΠ_h^*	Volume fraction m and angles at absolute maxΠ_h^*	Value of absolute maxΠ_h^*	Volume fraction m and angles at absolute maxΠ_h^*
d_h^*	228 pC/N	$m = 0.253$ and $\delta_x = 0°$, or $m = 0.253$ and $\delta_y = 0°$	372 pC/N	$m = 0.337$ and $\gamma = 90°$
g_h^*	230 mV· m/N	$m = 0.007$ and $\delta_x = 0°$, or $m = 0.007$ and $\delta_y = 0°$	284 mV· m/N	$m = 0.012$ and $\gamma = 90°$
e_h^*	24.3 C/m^2	$m = 0.811$ and $\delta_y = \pm 29°$	25.7 C/m^2	$m = 0.876$ and $\gamma = 90°$
$(Q_h^*)^2$	$15.3 \cdot 10^{-12}$ Pa^{-1}	$m = 0.038$ and $\delta_x = 0°$, or $m = 0.038$ and $\delta_y = 0°$	$33.8 \cdot 10^{-12}$ Pa^{-1}	$m = 0.068$ and $\gamma = 90°$
k_h^*	0.235	$m = 0.048$ and $\delta_x = 0°$, or $m = 0.048$ and $\delta_y = 0°$	0.361	$m = 0.095$ and $\gamma = 90°$

$$||d^*|| = \begin{pmatrix} 0 & 0 & 0 & 0 & d_{15}^* & 0 \\ 0 & 0 & 0 & d_{24}^* & 0 & 0 \\ d_{31}^* & d_{32}^* & d_{33}^* & 0 & 0 & 0 \end{pmatrix}. \tag{3.18}$$

A balance of d_{3j}^* in (3.18) promotes an increase of the hydrostatic piezoelectric coefficients d_h^*, g_h^*, and as a consequence, the squared hydrostatic figure of merit $(Q_h^*)^2$. In addition, the hydrostatic piezoelectric coefficient $d_h^{(1)}$ of the $[011]_c$-poled PMN–0.28PT SC at $\gamma = 0°$ is considerably more than $d_h^{(1)}$ in the $[111]_c$- and $[001]_c$-poled states.

3.2.2.2 Composites Based on PZN–0.07PT Single Crystals

The full set of electromechanical constants related to the $[011]_c$-poled relaxor-ferroelectric SC has first been measured [23] on PZN–0.07PT, a composition located near the MPB [20]. The PZN–0.07PT SC in the domain-engineered $[011]_c$-poled state (inset 3 in Fig. 3.6) is characterised [23] by *mm*2 symmetry and an unusual anisotropy of elastic and piezoelectric properties (cf. data from Tables 1.1 and 3.6). It is obvious that the symmetry and anisotropy of the properties differ from those particular to the $[001]_c$-poled PZN–*x*PT or PMN–*x*PT SCs. According to data from Table 3.6, the elastic compliances $s_{ab}^{(n),E}$ of the $[001]_c$-poled PZN–0.07PT SC are linked by ratios as follows:

$$s_{11}^{(n),E}/s_{12}^{(n),E} = -1.12, \quad s_{11}^{(n),E}/s_{13}^{(n),E} = 20.1 \text{ and } s_{11}^{(n),E}/s_{33}^{(n),E} = 1.09. \tag{3.19}$$

Ratios of the piezoelectric coefficients $d_{3j}^{(n)}$

$$d_{33}^{(n)}/d_{31}^{(n)} = 2.41 \text{ and } d_{33}^{(n)}/d_{32}^{(n)} = -0.788 \tag{3.20}$$

characterise the anisotropy of the piezoelectric effect in the same SC. We note that Eqs. (3.19) and (3.20) are related to the main crystallographic axes shown in inset 3 in Fig. 3.6. Ratios (3.19) and (3.20) differ from relations (3.16) and (3.17) which correspond to the $[011]_c$-poled PMN–0.28PT SC, and this circumstance is to be taken into account at the analysis of the effective parameters of the PZN–0.07PT-based composite.

It is assumed that the polydomain SC layers in the 2–2 composite (Fig. 3.10) represent crystal cuts with a clockwise rotation of the main crystallographic axes x and y around the co-ordinate axis $OX_3||$ z, where φ is the rotation angle. The composite sample is poled along the OX_3 axis. The macroscopic symmetry of the 2–2 composite based on the $[011]_c$-poled PZN–0.07PT SC enables us to consider a range of $0° \le \varphi \le 90°$ due to the condition $\Pi^*(m, \varphi) = \Pi^*(m, 180° - \varphi)$. The

Table 3.6 Elastic compliances $s_{ab}^{(n),E}$(in 10^{-12} Pa^{-1}), piezoelectric coefficients $d_{ij}^{(n)}$ (in pC/N) and dielectric permittivity $\varepsilon_{pp}^{(n),\sigma}$ of the domain-engineered $[011]_c$-poled PZN–0.07PT SC at room temperature [23]

$s_{11}^{(n),E}$	$s_{12}^{(n),E}$	$s_{13}^{(n),E}$	$s_{22}^{(n),E}$	$s_{23}^{(n),E}$	$s_{33}^{(n),E}$
67.52	–60.16	3.355	102.0	–54.47	62.02
$s_{44}^{(n),E}$	$s_{55}^{(n),E}$	$s_{66}^{(n),E}$	$d_{31}^{(n)}$	$d_{32}^{(n)}$	$d_{33}^{(n)}$
15.45	291.5	14.08	478	–1,460	1,150
$d_{15}^{(n)}$	$d_{24}^{(n)}$	$\varepsilon_{11}^{(n),\sigma}/\varepsilon_0$	$\varepsilon_{22}^{(n),\sigma}/\varepsilon_0$	$\varepsilon_{33}^{(n),\sigma}/\varepsilon_0$	
1,823	50	8,240	1,865	3,180	

Orientations of the spontaneous polarisation vectors in domains are shown in inset 3 in Fig. 3.6

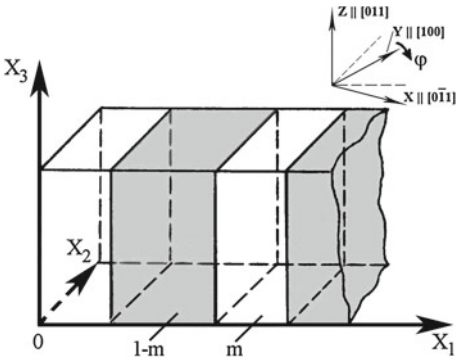

Fig. 3.10 Schematic of the 2–2 SC/polymer composite. $(X_1X_2X_3)$ is the rectangular co-ordinate system. m and $1 - m$ are volume fractions of the SC and polymer components, respectively, and φ is the angle of rotation of the main crystallographic axes x and y of the SC around the OX_3 axis (reprinted from paper by Krivoruchko and Topolov [30], with permission from IOP Publishing)

prediction of the effective properties and hydrostatic parameters of the composite is carried out using data from Tables 3.1 and 3.6. The matrix $||d^*||$ of the piezoelectric coefficients of the composite based on the $[011]_c$-poled PZN–0.07PT SC is given by (3.18).

Data on local maximum values $(\Pi^*)_m$ of the effective parameters at $\varphi = \text{const}$ (Table 3.7) characterise the piezoelectric response of the studied 2–2 composite. The piezoelectric anisotropy of the SC component [see, for instance, (3.19)] and its elastic anisotropy [see (3.20)] influence the orientation dependence of the effective parameters, such as g_{33}^*, g_h^*, $(Q_{33}^*)^2$, and $(Q_h^*)^2$. These parameters are concerned with the piezoelectric sensitivity of the composite and are increased by replacing araldite by a softer polymer. The presence of the very soft polymer (i.e., elastomer, see Table 3.1) in the composite leads to favourable changes in the piezoelectric coefficients d_{3j}^*, and these changes lead to an excellent hydrostatic piezoelectric activity of the composite (see Table 3.7 and curves 1–4 in Fig. 3.11a). Examples of the non-monotonic volume-fraction dependencies shown in Table 3.7 and Fig. 3.11 are closely connected with distinctions between the properties of the SC and polymer components as well as with a considerable redistribution of electric and mechanical fields in the 2–2 composite with interfaces $x_1 = \text{const}$ at the rotation mode shown in inset in Fig. 3.10.

We underline here the large changes in $(g_h^*)_m$ while there are relatively small changes in the related parameter $(g_{33}^*)_m$ (Table 3.7). Such behaviour is accounted for

Table 3.7 Local maximum values of the following effective parameters of the 2–2 $[011]_c$-poled PZN–0.07PT SC/polymer composite: piezoelectric coefficients $(g_{33}^*)_m$ (in mV·m/N), $(h_{33}^*)_m$ (in 10^8 V/m), $(e_{33}^*)_m$ (in C/m^2), hydrostatic piezoelectric coefficients d_h^* (in pC/N), $(g_h^*)_m$ (in mV·m/N), and squared figures of merit $(Q_{33}^*)_m^2$ (in 10^{-12} Pa^{-1}) and $(Q_h^*)_m^2$ (in 10^{-15} Pa^{-1})

Polymer	φ, deg	$(g_{33}^*)_m$	$(h_{33}^*)_m$	$(e_{33}^*)_m$	$(d_h^*)_m$	$(g_h^*)_m$	$(Q_{33}^*)_m^2$	$(Q_h^*)_m^2$
Araldite	0	499	34.4	7.88	–[a]	13.4	79.5	26.2
	15	493	33.0	7.67	–	−4.18	79.7	16.7
	30	457	26.5	7.42	–	8.08	81.2	152
	45	382	28.2	10.4	–	83.9	84.8	4,190
	60	426	38.2	13.1	–	187	84.5	1.28×10^4
	75	452	40.5	12.9	–	186	83.3	1.40×10^4
	90	458	41.0	12.8	–	184	83.0	1.39×10^4
Polyurethane	0	804	35.1	8.57	2.18	23.7	137	42.8
	15	795	33.6	8.30	0.318	5.34	137	42.2
	30	744	26.7	7.83	–	10.9	139	199
	45	640	28.3	11.5	–	136	143	6,970
	60	699	38.8	14.5	–	295	143	2.20×10^4
	75	737	41.1	14.1	–	297	141	2.48×10^4
	90	746	41.5	13.9	–	293	141	2.47×10^4
Elastomer	0	2,570	35.8	9.75	–	18.9	837	387
	15	2,560	34.2	9.38	–	5.97	864	153
	30	2,520	26.5	8.29	–	26.3	898	58.7
	45	2,410	27.1	14.5	–	235	917	9,510
	60	2,400	39.3	17.3	186	432	862	2.78×10^4
	75	2,430	41.8	16.1	224	445	825	3.30×10^4
	90	2,440	42.2	15.8	237	441	816	3.36×10^4

Reprinted from paper by Krivoruchko and Topolov [30], with permission from IOP Publishing
[a]The dash denotes monotonic increasing $d_h^*(m, \varphi)$ at $\varphi = \text{const}$

by changes in g_{31}^* and g_{32}^* as the main crystallographic axes x and y of SC undergo rotation (see inset in Fig. 3.10). The piezoelectric coefficients g_h^* and g_{33}^* demonstrate the possibilities of considerable increases in the sensitivity of the 2–2 composite at $\varphi \to 90°$ [30]: $(g_{33}^*)_m / g_{33}^{(1)} \approx 63$ and $(g_h^*)_m / g_h^{(1)} \approx 75$ where $g_{33}^{(1)}$ and $g_h^{(1)}$ are related to the main crystallographic axes of the $[011]_c$-poled PZN–0.07PT SC. The difference between $(g_{33}^*)_m$ and $(g_h^*)_m$ is associated with a change in a balance of the piezoelectric coefficients g_{3j}^* due to the piezoelectric coefficients $d_{3j}^{(1)}$ that obey conditions (3.20). In contrast to this result, the anisotropy of the elastic properties of the SC and the increase in softness of the polymer component lead to an increase in the piezoelectric coefficients h_{33}^* and e_{33}^*. In particular, the local maxima of $(h_{33}^*)_m$ and $(e_{33}^*)_m$ in a 2–2 $[011]_c$-poled PZN–0.07PT SC/elastomer composite become relatively large such that the ratios

$$(h_{33}^*)_m / h_{33}^{(1)} = 2.9 \text{ and } (e_{33}^*)_m / e_{33}^{(1)} = 4.7 \tag{3.21}$$

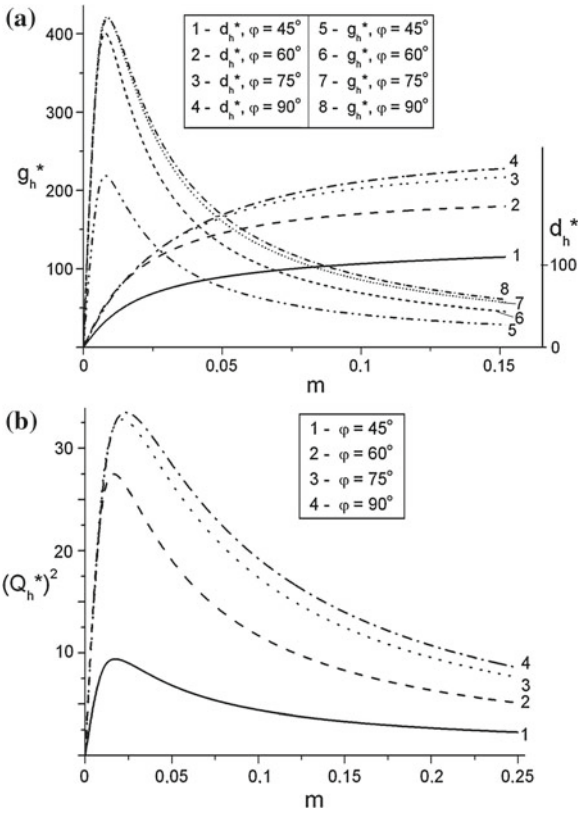

Fig. 3.11 Effective hydrostatic parameters of the 2–2 $[011]_c$-poled PZN–0.07PT SC/elastomer composite: piezoelectric coefficients d_h^* (**a**, in pC/N) and g_h^* (**a**, in mV· m/N) and squared figure of merit $(Q_h^*)^2$ (**b**, in 10^{-12} Pa^{-1}) (reprinted from paper by Krivoruchko and Topolov [30], with permission from IOP Publishing)

are valid [30], where $h_{33}^{(1)}$ and $e_{33}^{(1)}$ are related to the main crystallographic axes. A distinction between the volume-fraction dependences of h_{33}^* and e_{33}^* at φ = const is associated with dielectric permittivity $\varepsilon_{33}^{*\xi}$ that increases monotonously with increasing m. These large values of ratios (3.21) have first been mentioned [30] in research on the piezoelectric coefficients h_{33}^* and e_{33}^* of 2–2 relaxor-ferroelectric SC/polymer composites. We note for comparison that 1–β PZT-type FC/elastomer composites (β = 1, 2 or 3) are characterised by max $e_{33}^*/e_{33}^{(1)} \approx 1.1 - 1.2$ [2, 32] where e_{33}^* is a function of the volume fraction of FC, and $e_{33}^{(1)}$ is its piezoelectric coefficient.

The high piezoelectric activity of 2–2 composites based on $[011]_c$-poled PZN–0.07PT SC at small m values (see curves 1–4 in Fig. 3.11a) favours high piezoelectric sensitivity (see curves 5–8 in Fig. 3.11a and curves 1–4 in Fig. 3.11b). The hydrostatic parameters g_h^* and $(Q_h^*)^2$ at the ranges $0.01 < m < 0.10$ and $45° < \varphi < 90°$

(Fig. 3.11) are a few times larger than $\max g_h^*$ and $\max(Q_h^*)^2$ which are known [2, 11] for 2–2 parallel-connected FC/polymer composites.

The advantages of 2–2 composites based on $[011]_c$-poled PZN–0.07PT SC stem from the interconnection between the piezoelectric activity and sensitivity [30] and should be taken into consideration when manufacturing novel 2–2-type piezo-active composites.

3.2.3 *Change in the Poling Orientation of Ferroelectric Polymer: An Additional Orientation Effect*

Now we replace the PVDF-1 layers with the PVDF-2 layers over the 2–2 composite sample. The remanent polarisation vector $\boldsymbol{P}_r^{(2)}$ in the PVDF-2 layer is shown in inset 5 in Fig. 3.6: it is clear that this layer has been poled in the opposite direction (see inset 4 in Fig. 3.6) to the aforementioned PVDF-1 layer. The change in the poling direction of the ferroelectric polymer results in opposite signs of the piezoelectric coefficients of PVDF-2 in comparison to PVDF-1, and this effect can be taken into account in the subsequent consideration of the effective parameters of the composite. Negative values of $d_{33}^{(2)}$, $e_{33}^{(2)}$ and $g_{33}^{(2)}$ influence the volume-fraction dependence of g_{33}^*, g_h^* etc., however the change in the $\boldsymbol{P}_r^{(2)}$ direction does not give rise to considerable changes in the orientation dependence of the effective parameters of the 2–2 composite. Data on the 2–2 composite based on the single-domain PMN–0.33PT SC (Table 3.8) show that maximum (or minimum) values of the effective parameters related to small volume fractions of the SC component ($m \ll 1$) undergo considerable changes due to the influence of the piezoelectric and dielectric properties of the polymer component. It should be remembered that the piezoelectric coefficient $d_{33}^{(2)}$ of PVDF is about four times less than $d_{33}^{(1)}$ of the single-domain PMN–0.33PT SC (cf. data from Tables 2.1 and 3.3) and may play an important role in determining the electromechanical properties of the composite even at $m \approx 1/4$. Changes in the value of $(Q_h^*)^2$ (Table 3.8) are caused not only by the changes in signs of $d_{3j}^{(2)}$ and $g_{3j}^{(2)}$, but also by a shift of the volume fraction m, at which absolute $\max(Q_h^*)^2$ is achieved, to lower values. This means that the hydrostatic piezoelectric coefficient g_h^* plays the dominant role in forming the volume-fraction dependence of $(Q_h^*)^2$.

The value of absolute min e_h^* undergoes very minor changes at the transition from the composite with the PVDF-1 layers to the composite with the PVDF-2 layers (Table 3.8). The volume faction $m \approx 0.83$ at which absolute min e_h^* is achieved in both the composites demonstrates the key role of the SC component in forming the piezoelectric performance of the composites. Similar changes in max e_{33}^* are observed at $m \approx 0.97$ (Table 3.8) and, therefore, a weak influence of the polymer component on the longitudinal piezoelectric response of the composite is expected.

An important example of changes in the composite performance is concerned with three orientations of the remanent polarisation vector $\boldsymbol{P}_r^{(2)}$ in the polymer layers. It

Table 3.8 Absolute maxima (minima) of longitudinal and hydrostatic parameters of the 2–2 single-domain PMN–0.33PT SC/PVDF-2 composite in comparison to the 2–2 single-domain PMN–0.33PT SC/PVDF-1 composite

	Composite with PVDF-2 layers[a]		Composite with PVDF-1 layers[b]
Π^*	Value of absolute max Π^* (or min Π^*)	m, φ, ψ, and θ which correspond to the value of absolute max Π^* (or min Π^*)	Value of absolute max Π^* (or min Π^*)
g_{33}^*	-605 mV·m/N[c]	$m = 0.020$, $\varphi = 0°$, $\psi = 0°$, and $\theta = 106°$	539 mV· m/N
e_{33}^*	12.4 C/m^2	$m = 0.969$, $\varphi = 0°$, $\psi = 0°$, and $\theta = 0°$	12.4 C/m^2
d_h^*	-327 pC/N[c]	$m = 0.303$, $\varphi = 0°$, $\psi = 0°$, and $\theta = 86°$	-322 pC/N[c]
g_h^*	-305 mV·m/N[c]	$m = 0.015$, $\varphi = 60°$, $\psi = 90°$, and $\theta = 127°$	-252 mV·m/N[c]
e_h^*	-22.4 C/m^2[c]	$m = 0.831$, $\varphi = 60°$, $\psi = 90°$, and $\theta = 117°$	-22.3 C/m^2[c]
$(Q_h^*)^2$	$23.8 \cdot 10^{-12}$ Pa^{-1}	$m = 0.055$, $\varphi = 60°$, $\psi = 90°$, and $\theta = 124°$	$21.5 \cdot 10^{-12}$Pa^{-1}
k_h^*	-0.304[c]	$m = 0.071$, $\varphi = 60°$, $\psi = 90°$, and $\theta = 124°$	0.294

[a] Orientations of $\mathbf{P}_r^{(2)}$ and $\mathbf{P}_s^{(1)}$ are shown in Fig. 3.6, see insets 1 and 5, respectively

[b] Orientations of $\mathbf{P}_r^{(2)}$ and $\mathbf{P}_s^{(1)}$ are shown in Fig. 3.6, see insets 1 and 4, respectively

[c] Absolute minimum value

is assumed that the 2–2 composite contains layers of the $[011]_c$-poled PZN–0.07PT SC and PVDF, and the remanent polarisation vector $\boldsymbol{P}_r^{(2)}$ in PVDF is oriented as follows:

(i) $\boldsymbol{P}_r^{(2)}$ $\uparrow\downarrow OX_3$ (PVDF-1),
(ii) $\boldsymbol{P}_r^{(2)}$ $\uparrow\uparrow OX_3$ (PVDF-2) or
(iii) $\boldsymbol{P}_r^{(2)}$ $\uparrow\uparrow OX_2$ (PVDF-p).

The main crystallographic axes in each SC layer rotate as shown in the inset in Fig. 3.10.

The PZN–0.07PT-based composite shows high hydrostatic piezoelectric activity (Fig.3.12a–c): values of max $d_h^* = 2.26 d_h^{(1)}$, max $d_h^* = 2.06 d_h^{(1)}$ and max $d_h^* = 2.28 d_h^{(1)}$ are achieved in the presence of the PVDF-2, PVDF-p and PVDF-1 layers, respectively. The minor changes in max d_h^* values are also accounted for by a slight influence of the polymer component (and, therefore, the orientation of the poling axis therein) on the piezoelectric coefficients d_{3j}^* at $m \approx 0.4$–0.5. The max d_h^* values found for the PZN–0.07PT-based composite [31] are about 5–6 times more than max d_h^* of the 2–2 PZT-type FC/polymer composites [11]. The max g_h^* values related to the PZN–0.07PT-based composite are about 1.5–2 times more than max g_h^* of the 2–2 PZT-type FC/polymer composites [11], and as in the 2–2 SC/polymer composites, max g_h^* is achieved at relatively small volume fractions ($m \ll 1$) of the SC component. Changes in graphs of g_h^* and $(Q_h^*)^2$ become distinct at $0 < m < 0.1$ (Fig.3.12d–i), since the piezoelectric and dielectric properties of the PVDF layers have a strong influence on the performance of the 2–2 composite, irrespective of the $\boldsymbol{P}_r^{(2)}$ orientation in these layers.

Thus, the above-described orientation effect concerned with the orientation of the remanent polarisation vector $\boldsymbol{P}_r^{(2)}$ in ferroelectric polymer layers (see insets 4 and 5 in Fig. 3.6) may be regarded as an additional effect that would lead to major changes in the effective parameters of the 2–2 composite at volume fractions of SC $0 < m < 0.1$ only.

3.2.4 Composites with Auxetic Polymer Components

In this section we discuss an effect of the elastic properties of the polymer layers on the piezoelectric anisotropy and hydrostatic parameters of the composite. Among the polymer components of interest, we choose for comparison a monolithic polyurethane (a conventional isotropic polymer with a Poisson's ratio $\nu^{(n)} = -s_{12}^{(n)}/s_{11}^{(n)} = 0.37$, see constants in Table 3.1) and an auxetic polyethylene (PE) with the negative Poisson's ratio $\nu^{(n)} = -0.83$.[1] The presence of an auxetic polymer component enables us

[1] According to experimental data [33], this piezo-passive auxetic polymer is characterised by elastic compliances $s_{11}^{(n)} = 5,260$ and $s_{12}^{(n)} = 4,360$ (in 10^{-12} Pa^{-1}) and dielectric permittivity $\varepsilon_{pp}^{(n)}/\varepsilon_0 = 2.3$ at room temperature. We add that an effect of the auxetic polymer on the perfor-

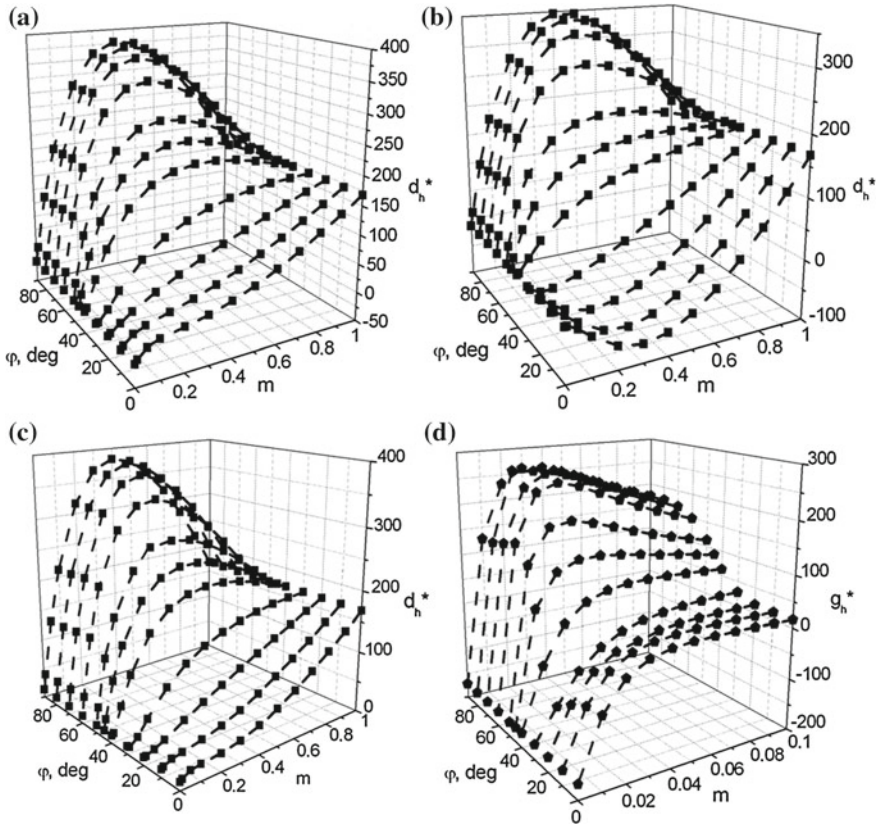

Fig. 3.12 Effective hydrostatic parameters of a 2–2 $[011]_c$-poled PZN–0.07PT SC/PVDF composite with layers of PVDF-2 (**a**, **d**, **g**), PVDF-p (**b**, **e**, **h**), or PVDF-1 (**c**, **f**, **i**): d_h^* (**a**–**c**, in pC/N), g_h^* (**d**–**f**, in mV·m/N) and $(Q_h^*)^2$ (**g**–**i**, in 10^{-12} Pa^{-1}) (reprinted from paper by and Topolov and Krivoruchko [31] with permission from the American Institute of Physics)

to characterise the laminar composite as a simple 2–2 type composite, without details in connectivity of the polymer layers. In Sect. 2.4 we considered the performance of the single-domain relaxor-ferroelectric PIN–*x*–*y* SCs, and the following compositions are now considered as components of the studied composite: PIN–0.24–0.49 (3*m* symmetry) and PIN–0.27–0.40 (*mm*2 symmetry) [34, 35]. It is assumed that the SC/polymer composite has a regular laminar structure with interfaces $x_1 = \text{const}$, and the orientation of the crystallographic axes and the spontaneous polarisation vector $\boldsymbol{P}_s^{(1)}$ in each SC layer is shown in inset 1 in Fig. 3.6. As earlier, we assume that the electrodes are perpendicular to the OX_3 axis.

mance of the 1–3-type piezo-active composites is discussed in Sect. 4.3.4 where variations of the elastic properties of the auxetic polymer component are taken into account.

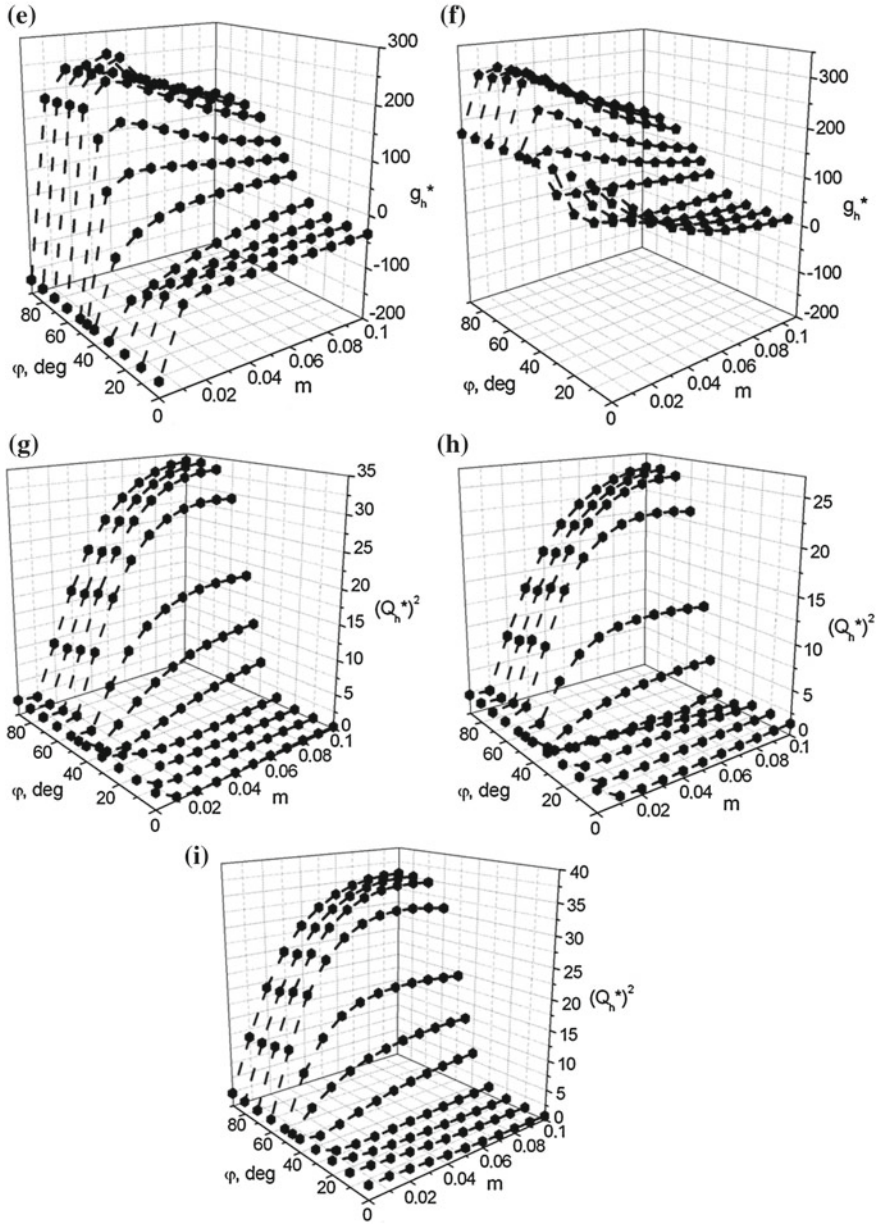

Fig. 3.12 (continued)

3.2.4.1 Anisotropy Factors

As follows from a comparison of the sets of electromechanical constants of single-domain PIN–*x*–*y* SCs (Table 2.3), the PIN–0.24–0.49 SC exhibits a larger anisotropy of piezoelectric coefficients $d_{3j}^{(1)}$ and ECFs $k_{3j}^{(1)}$ so that the ratios $d_{33}^{(1)}/d_{31}^{(1)} = -3.6$ and $k_{33}^{(1)}/k_{31}^{(1)} = -4.9$ hold. By analogy with these ratios we consider the anisotropy factors ζ_{d3j} from (3.8) and

$$\zeta_{k31} = k_{33}^{*}/k_{31}^{*} \text{ and } \zeta_{k32} = k_{33}^{*}/k_{32}^{*} \tag{3.22}$$

where the ECFs k_{3j}^{*} of the composite are determined with relations similar to (1.21) and (1.22):

$$k_{3j}^{*} = d_{3j}^{*}/(\varepsilon_{33}^{*\sigma} s_{jj}^{*E})^{1/2} \tag{3.23}$$

where $j = 1$, 2 and 3. Taking into account (3.8) and (3.23), we represent ζ_{k3j} from (3.22) as

$$\zeta_{k31} = \zeta_{d31}(s_{11}^{*E}/s_{33}^{*E})^{1/2} \text{ and } \zeta_{k32} = \zeta_{d32}(s_{22}^{*E}/s_{33}^{*E})^{1/2}. \tag{3.24}$$

Hereafter we consider the conditions for a large anisotropy of d_{3j}^{*} and k_{3j}^{*} of the composite in the following form:

$$|\zeta_{d31}| \geq 10 \text{ and } |\zeta_{d32}| \geq 10 \tag{3.25}$$

and

$$|\zeta_{k31}| \geq 10 \text{ and } |\zeta_{k32}| \geq 10, \tag{3.26}$$

respectively.

From our analysis of the volume-fraction and orientation dependences of the piezoelectric coefficients d_{3j}^{*} and ECFs k_{3j}^{*}, we observe that both conditions (3.25) and (3.26) are not valid in polyurethane-containing composites. Replacing the polyurethane layers with an auxetic PE enables us to find regions of validity of conditions (3.25) and (3.26) (Fig.3.13). For the PIN–0.24–0.49-based composite with a larger anisotropy of $d_{3j}^{(1)}$ and $k_{3j}^{(1)}$, conditions (3.25) and (3.26) are valid (Fig.3.13a) even when only varying the Euler angle θ (see inset in Fig. 3.1). Changes in the orientation of the main crystallographic axes of the single- domain SC with 3*m* symmetry are related to the rotation of the spontaneous polarisation vector $\boldsymbol{P}_{\boldsymbol{s}}^{(1)}$ with respect to the OX_3 axis (see inset 1 in Fig. 3.6). We note that the smaller regions of the simultaneous fulfilment of conditions (3.25) and (3.26) are achieved in the PIN–0.27–0.40-based composite (Fig. 3.13c, d). Such a response can be accounted for by the smaller anisotropy of $d_{3j}^{(1)}$, $s_{ab}^{(1),E}$ and $k_{3j}^{(1)}$ in the single-domain PIN–0.27–0.40

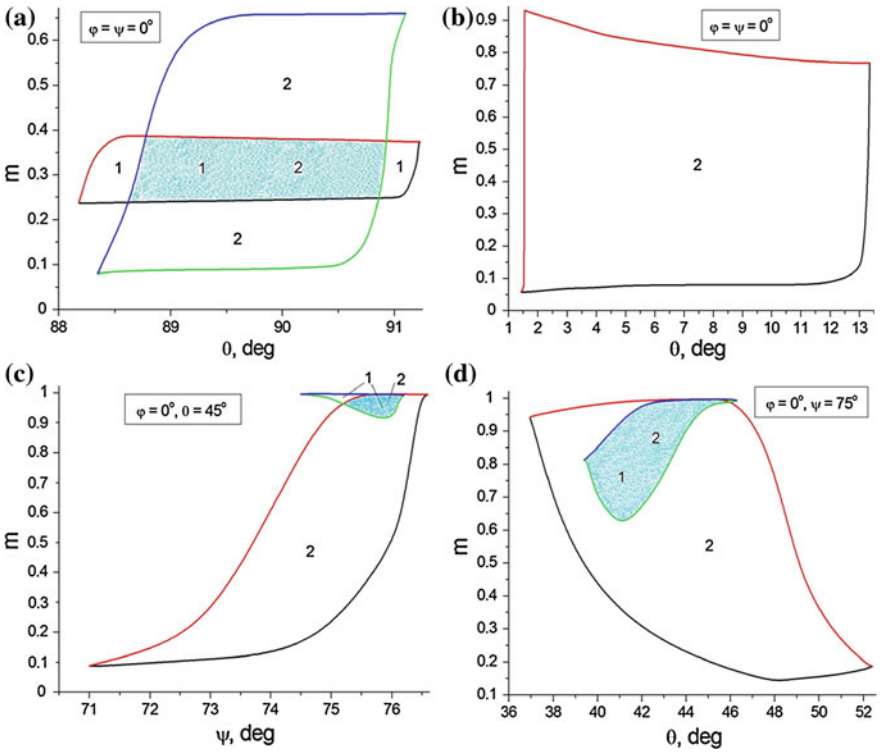

Fig. 3.13 Regions of the large anisotropy of d^*_{3j} and k^*_{3j} in a 2–2 single-domain PIN–0.24–0.49 SC/auxetic PE composite (**a**, **b**) and in a 2–2 single-domain PIN–0.27–0.40 SC/auxetic PE composite (**c**, **d**) at variations of the Euler angle θ (see inset 1 in Fig. 3.5). Conditions (3.25) are valid in region 1, and conditions (3.26) are valid in region 2. Filled areas in graphs (**a**), (**c**), (**d**) are related to the simultaneous fulfilment of conditions (3.25) and (3.26) (reprinted from paper by Topolov et al. [36], with permission from Wiley-VCH Verlag)

SC with *mm*2 symmetry. Irrespective of the SC component, the use of an auxetic polymer component promotes a larger piezoelectric anisotropy due to the unusual strain and the re-distribution of internal elastic and electric fields in the composite.

It is important to highlight that conditions (3.25) and (3.26) are valid at volume fractions m, for which the piezoelectric coefficient $d^*_{33}\ (m, \varphi, \psi, \theta) \approx d^{(1)}_{33}$ and ECF $k^*_{33}\ (m, \varphi, \psi, \theta) \approx 0.6$ [36]. The orientation dependence of the electromechanical properties of the SC component plays an important role in achieving a large piezoelectric anisotropy. According to results [36], the piezoelectric coefficient $d^{(1)}_{33}$, elastic compliance $s^{(1),E}_{33}$ and ECF $k^{(1)}_{33}$ of single-domain PIN–0.24–0.49 SC undergo large changes upon varying the angle θ. The 2–2 single-domain PIN–0.24–0.49 SC/auxetic PE composite shows some advantages over well-known FCs based on $PbTiO_3$ [17] due to larger values of d^*_{33} and k^*_{33} in regions where the conditions (3.25) and (3.26)

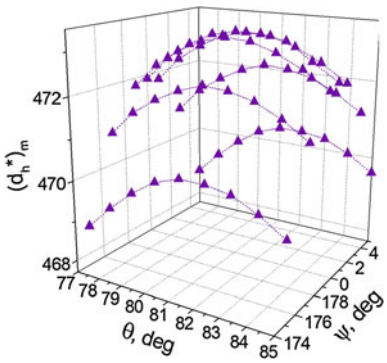

Fig. 3.14 Local maxima of the hydrostatic piezoelectric coefficient $(d_h^*)_m$ (in pC/N) in the 2–2 single-domain PIN–0.24–0.49 SC/auxetic PE composite near absolute max d_h^*. This graph was built at $\varphi = 0°$ (reprinted from paper by Topolov et al. [36], with permission from Wiley-VCH Verlag)

are valid, and this performance is important in piezo-technical applications such as actuators, transducers, acoustic antennae based on pulse-echo principles.

3.2.4.2 Hydrostatic Parameters

The hydrostatic parameters (3.2) and (3.3) are highly dependent on the anisotropy factors ζ_{d3j} from (3.8) and vary in a wide range when changing m, φ, ψ, and θ [36]. An increase in the hydrostatic parameters of the composite is observed by replacing the conventional polymer layers with an auxetic polymer. Figure 3.14 shows, that even in the presence of a single-domain PIN–0.24–0.49 SC with $d_h^{(1)}$ = 33 pC/N [34], a considerable increase in the effective hydrostatic piezoelectric coefficient d_h^* of the composite is expected. A value of absolute max d_h^* $(m, \varphi, \psi, \theta)$ = 473 pC/N $\approx 14.3\ d_h^{(1)}$ [36] is found at $m = 0.188$, $\varphi = \psi = 0°$ and $\theta = 81°$. The 2–2 single-domain PIN–0.24–0.49 SC/auxetic PE composite is characterised by large values of absolute maxima of g_h^* and $(Q_h^*)^2$, however these maxima are observed at very low volume fractions of SC. According to work [36], absolute max$g_h^*(m, \varphi, \psi, \theta)$ = 3,860 mV· m/N can be achieved at $m_{gh} = 0.0008$, and absolute max$[Q_h^*(m, \varphi, \psi, \theta)]^2$ = $1.71 \cdot 10^{-9}$ Pa^{-1} is achieved at $m_{Qh} = 0.0014$. This is due to the large elastic compliances of the auxetic component [33] as compared to the SC and by the influence of the dielectric properties of the polymer component [2] on the non-monotonic behaviour of g_h^* and $(Q_h^*)^2$ at $m \ll 1$. It is obvious that the aforementioned volume fractions $0 < m_{gh} < 0.01$ and $0 < m_{Qh} < 0.01$ make it difficult to manufacture a composite sample with extremely high values of g_h^* and $(Q_h^*)^2$. To avoid this weak spot in the performance of the novel 2–2-type composite, we consider local maxima of its hydrostatic parameters (3.2) and (3.3) at larger volume fractions of SC, namely, at $m = 0.05$ (Fig. 3.15) and $m = 0.10$ (Fig. 3.16).

The large decrease of g_h^* (Figs. 3.15a and 3.16a) and $(Q_h^*)^2$(Figs. 3.15b and 3.16b) in comparison to the aforementioned values of absolute max g_h^* $(m, \varphi, \psi, \theta)$ and max$[Q_h^*(m, \varphi, \psi, \theta)]^2$, respectively, is due to the increasing dielectric permittivity

$\varepsilon_{33}^{*\sigma}$. At $0.05 \leq m \leq 0.10$ the inequality $\varepsilon_{33}^{*\sigma} \ll \varepsilon_{33}^{(1),\sigma}$ holds, and this feature favours relatively large values of $g_h^* \sim 10^2$ mV·m/N (Figs.3.15a, d, and 3.16a, d) and $(Q_h^*)^2 \sim 10^{-11} - 10^{-10}$ Pa^{-1} (Figs. 3.15b and 3.16b) which are of interest for hydroacoustic applications. It should be added that the relatively large absolute value of the hydrostatic piezoelectric coefficient $|d_h^*| \sim 10^2$ pC/N (Figs. 3.15c and 3.16c) is due to the rapid increase of $|d_{3j}^*|$ in the presence of the soft auxetic polymer layers, and this increase also favours large values of $(Q_h^*)^2$ in accordance with (3.2) and (3.3). Values of $d_h^* < 0$ and $g_h^* < 0$ (Figs. 3.15c, d and 3.16c, d) are accounted for by the dependence of the hydrostatic response of the composite on the Euler angle $90° < \theta < 180°$: at such orientations a negative projection of the spontaneous polarisation vector $\boldsymbol{P}_s^{(1)}$ onto the OX_3 axis (see inset 1 in Fig. 3.6) promotes $d_{33}^* < 0$ that has a strong influence on the balance of d_{3j}^* in (3.2) and therefore sgn d_h^* respect to the poling direction [3].

Thus, the 2–2 relaxor-ferroelectic SC/auxetic polymer composites demonstrate important advantages over the conventional 2–2 FC/polymer composites due to the large piezoelectric anisotropy, hydrostatic parameters etc. The dominating effect, that causes these advantages, is the elastic properties of the SC and auxetic polymer components at the strong influence of the rotation of the crystallographic axes of the single-domain SC component on the elastic and piezoelectric anisotropy. The composite performance discussed in Sects. 3.2.4.1 and 3.2.4.2 is of value for transducer, sensor, hydroacoustic, and other applications.

It should be noted that values of $(Q_h^*)^2$ of the 2–2 single-domain PIN–0.24–0.49 SC/auxetic PE composite at $m = 0.05$ (Fig. 3.15b) and 0.10 (Fig. 3.16b) remain much more than absolute $\max[Q_h^*(m, \varphi, \psi, \theta)]^2$ of the composites with polyurethane layers [36]. The PIN–0.24–0.49 SC/polyurethane and PIN–0.27–0.40/polyurethane composites are characterised by max d_h^* [36] that are comparable to local max d_h^* of the PIN–0.24–0.49/auxetic PE composite at $m = 0.05$ (Fig. 3.15c) and 0.10 (Fig. 3.16c), however these volume fractions of SC are much less than $m \approx 0.3$ related to max d_h^* in the aforementioned polyurethane-containing composites. This clear difference in the volume fractions m is also one of the advantages of the 2–2 single-domain PIN–0.24–0.49 SC/auxetic PE composite over the related SC/polyurethane composites [36].

Evaluating the performance of the PIN–0.24–0.49-based composite, one can underline that the presence of an auxetic polymer leads to obvious advantages of this composite over the PZT-type FC/conventional polymer composites with typical values of max$d_h^* \approx$ (50–80) pC/N and max$g_h^* \approx$ (100–300) mV·m/N [2, 11]. We add for comparison that an experimental value of $\max(Q_h^*)^2 \approx 5 \cdot 10^{-11}$ Pa^{-1} (i.e., about 3 times lower than the $(Q_h^*)^2$ values in Fig. 3.15b) can be achieved in a 2–2 PZT-type FC/polymer composite with a specific orientation of the FC layers.

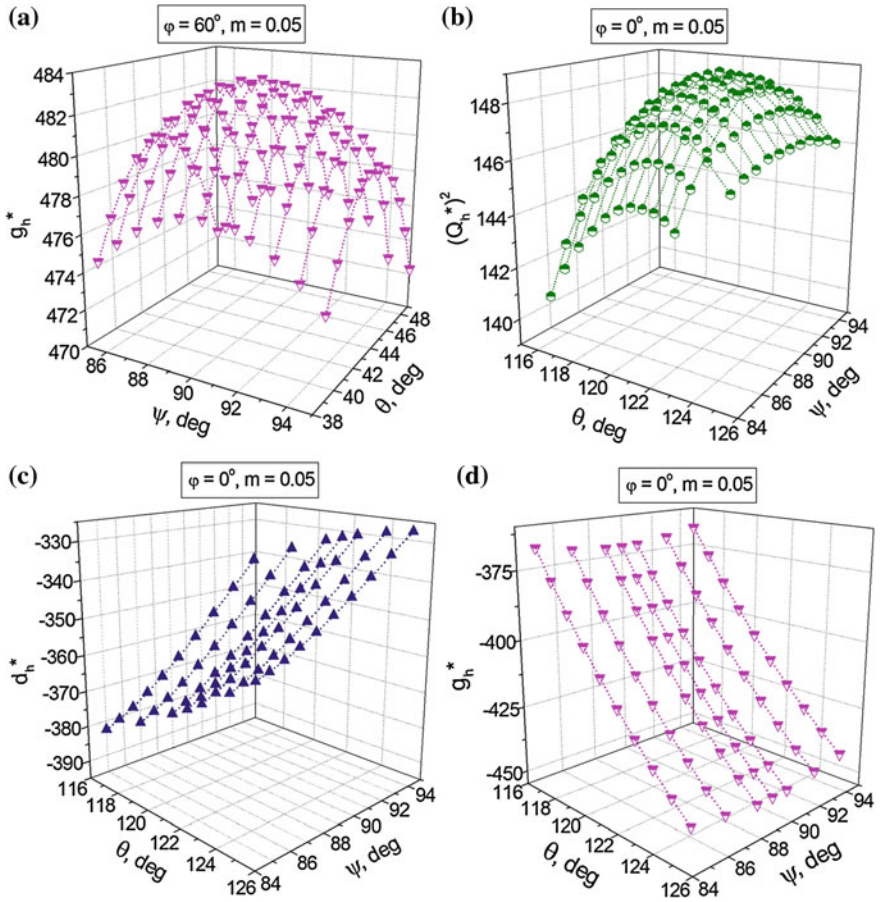

Fig. 3.15 Hydrostatic parameters of the 2–2 single-domain PIN–0.24–0.49 SC/auxetic PE composite in the vicinity of local max g_h^* (**a**) and max$[(Q_h^*)^2]$ (**b**–**d**) at $m = 0.05$: g_h^*(in mV·m/N, **a**, **d**), $(Q_h^*)^2$ (in 10^{-12} Pa^{-1}, **b**) and d_h^* (in pC/N, **c**) (reprinted from paper by Topolov et al. [36], with permission from Wiley-VCH Verlag)

3.3 2–2–0 Composites with Porous Polymer Matrices

In this section we consider a porous structure within the polymer layers and the influence of porosity on the effective parameters of the 2–2-type composite. It is now assumed that the composite sample (Fig. 3.17) contains a system of parallel layers which are made from relaxor-ferroelectric SC and porous polymer and are alternating in the OX_1 direction. These layers are assumed to be continuous along the OX_2 and OX_3 axes of the rectangular co-ordinate system $(X_1X_2X_3)$. The main crystallographic axes x, y and z in each SC layer are oriented as shown in inset 1 in Fig. 3.17.

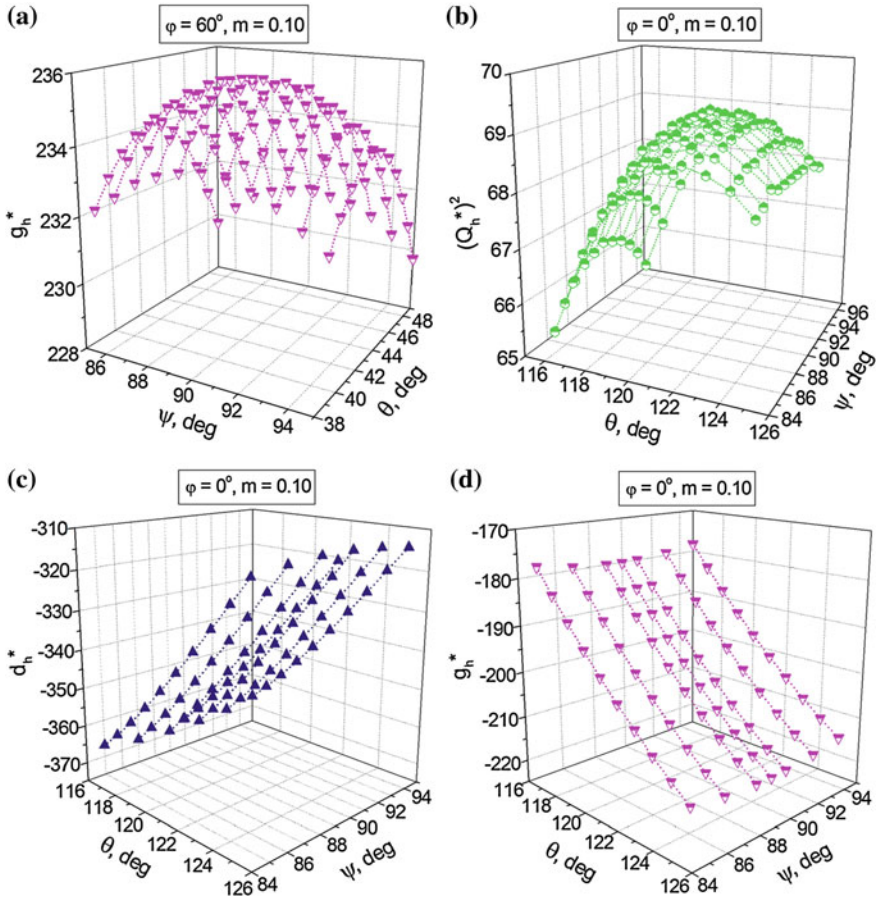

Fig. 3.16 Hydrostatic parameters of the 2–2 single-domain PIN–0.24–0.49 SC/auxetic PE composite in the vicinity of local maxg_h^* (**a**) and max$[(Q_h^*)^2]$ (**b**–**d**) at $m = 0.10$: g_h^* (in mV·m/N, **a** and **d**), $(Q_h^*)^2$(in 10^{-12} Pa^{-1}, **b**) and d_h^* (in pC/N, **c**) (reprinted from paper by Topolov et al. [36], with permission from Wiley-VCH Verlag)

Each polymer layer contains a systems of isolated air pores and can be regarded as a porous material P-*k* with 3–0 connectivity. Hereafter we consider the following porous structures:

(i) spherical pores distributed randomly in the matrix (P-1, see inset 2 in Fig. 3.17),
(ii) oblate spheroidal air pores that are regularly distributed and described by an equation

$$(x_1/a_1)^2 + (x_2/a_2)^2 + (x_3/a_3)^2 = 1 \tag{3.27}$$

in the $(X_1X_2X_3)$ system. Semi-axes a_i in (3.27) are linked by one of the aspect ratios – either $\rho_1 = a_3/a_1 = a_3/a_2 < 1$ (P-2, see inset 3 in Fig. 3.17) or $\rho_2 = a_1/a_2 = a_1/a_3 < 1$ (P-3, see inset 4 in Fig. 3.17). The corresponding composite with any porous matrix P-*k* (insets 2–4 in Fig. 3.17) represents examples of 2–2–0 connectivity. The air pores in the polymer layers are characterised by the volume fraction (porosity) m_p, and the sizes of these pores are considerably less than the thickness of the polymer layer in the OX_1 direction. This assumption on the sizes enables us to determine the effective electromechanical properties in the 2–2–0 composite in two stages. At the first stage calculating the effective constants of the porous polymer P-*k* at various m_p and ρ_i $(i = 1\,or\,2)$ is performed using formulae [37, 38]. At the second stage the effective electromechanical properties of the composite are determined by means of the matrix method applied to the 2–2 composite [see (3.4) and (3.5)]. The effective properties and related parameters of the 2–2–0 composite are represented in the general form as $\Pi^*(m, \varphi, m_p, \rho_i)$. For a composite with the P-1 layers (see inset 2 in Fig. 3.17), a condition $\rho_1 = \rho_2 = 1$ holds.

Forming the porous structure in the polymer matrix leads to a large increase of the hydrostatic piezoelectric coefficient g_h^*, squared figures of merit $(Q_{33}^*)^2$ and $(Q_h^*)^2$ etc. It is seen that local maxima of $(g_h^*)_m$(curves 2, 4 and 6 in Fig. 3.18a), $(Q_{33}^*)_m^2$ and $(Q_h^*)_m^2$ (Fig. 3.18b) in the 2–2–0 composite become larger than similar parameters of the related 2–2 composite (see Fig. 3.11 and Table 3.7). The increase in $(d_h^*)_m$(curves 1, 3 and 5 in Fig. 3.18a) is less pronounced. This feature of the composite is a result of a decrease of the elastic moduli $c_{ab}^{(2)}$ of the porous polymer and with a change in ratios of diagonal $(a = b)$ and off-diagonal $(a \neq b)$ elastic moduli $c_{ab}^{(2)}$, however

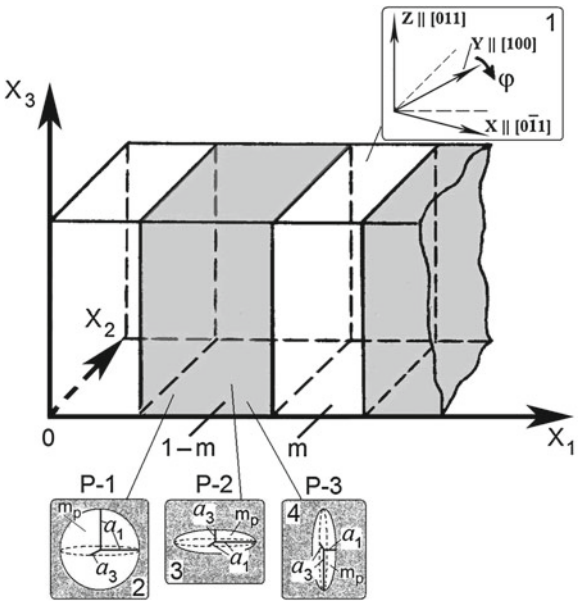

Fig. 3.17 Schematic of the 2–2–0 SC/porous polymer composite. $(X_1X_2X_3)$ is the rectangular co-ordinate system. m and $1 - m$ are volume fractions of the SC and porous polymer components, respectively. In *inset* 1 φ is the angle of rotation of the main crystallographic axes x and y of the SC layer around the OX_3 axis. In *insets* 2–4 a_i are semi-axes of the spheroidal air pore, and m_p is porosity in the polymer layer

in the porous polymers P-k their elastic moduli remains much smaller than those of the SC component. The porous structure of the polymer layer influences the balance of the piezoelectric coefficients d^*_{3j} that lead to a change in the relations between $(Q^*_{33})^2_m$ and $(Q^*_h)^2_m$ (compare curves 1, 3 and 5 with curves 2, 4 and 6, respectively, in Fig. 3.18b). Fig. 3.18a and curves 2, 4 and 6 in Fig. 3.18b suggest that the largest values of the three hydrostatic parameters, d^*_h, g^*_h and $(Q^*_h)^2$, are attained in the 2–2–0 composite in the vicinity of $\varphi = 90°$ irrespective of the porous material P-k. Such an orientation of the main crystallographic axes of the SC layer (see inset 1 in Fig. 3.17) weakens the influence of the negative piezoelectric coefficient $d^{(1)}_{32}$ of the $[011]_c$-poled PZN–0.07PT SC and strengthens an influence of the positive piezoelectric coefficient $d^{(1)}_{31}$ on the hydrostatic response of the 2–2–0 composite. In particular, the 2–2–0 composite with P-2 is characterised by the largest $(Q^*_{33})^2$ values (see Fig. 3.18c and curve 3 in Fig. 3.18b). The presence of oblate spheroidal pores with $\rho_1 < 1$ and an equality of the piezoelectric coefficients $d^{(1)}_{31} = d^{(1)}_{32}$ in the SC layer at $\varphi = 45°$ are regarded as the main factors that favour an appreciable increase of the piezoelectric sensitivity of the 2–2–0 composite along the OX_3 axis.

The increase of $(Q^*_h)^2$ at $45° < \varphi < 90°$ (see Fig. 3.18d) is due to the influence of the piezoelectric coefficients $d^{(1)}_{31}$ and $d^{(1)}_{32}$ of the SC layer on the hydrostatic response of the 2–2–0 composite. Such an increase has obvious advantages: even when increasing the volume fraction m by 0.05 (see curve 4 in Fig. 3.18d) the $(Q^*_h)^2$ value at $\varphi = 90°$ is about five times more than $\max[(Q^*_h)^2]$ of the oriented 2–2 FC/polymer composite [3]. A relatively slow decrease of $(Q^*_h)^2$ with increasing m (as $\max[(Q^*_h)^2]$ is passed, see curves 2–4 in Fig. 3.18d) and at $\varphi > 45°$ is associated with the favourable balance of the piezoelectric coefficients $d^{(1)}_{3j}$ of the $[011]_c$-poled PZN–0.07PT SC (see Table 3.6) and with the smaller differences $c^{(1),E}_{ab} - c^{(2)}_{ab}$ related to the 2–2–0 composite with P-2.

Thus, as with an auxetic polymer layer, the use of a porous polymer layer (expecially P-2) promotes a high piezoelectric sensitivity and an increase of the hydrostatic parameters (3.1)–(3.3) of the 2–2–0 composite (Fig. 3.17) at the appropriate orientation of the main crystallographic axes of the SC component. The values of $(Q^*_{33})^2$ and $(Q^*_h)^2$ remain fairly large after passing the maxima points and increasing the volume fraction m by 5 % (Fig. 3.18c, d). Such a performance is of value for sensor, hydrophone and other potential applications of the 2–2–0 SC/porous polymer composite. The aspect ratios ρ_i of the air pores also influence the effective parameters of the composite [30], and replacing the P-2 layer with the P-3 layer at $m_p = \text{const}$ means an orientation effect is to be taken into account for the prediction of the optimum performance of these novel piezo-active composites.

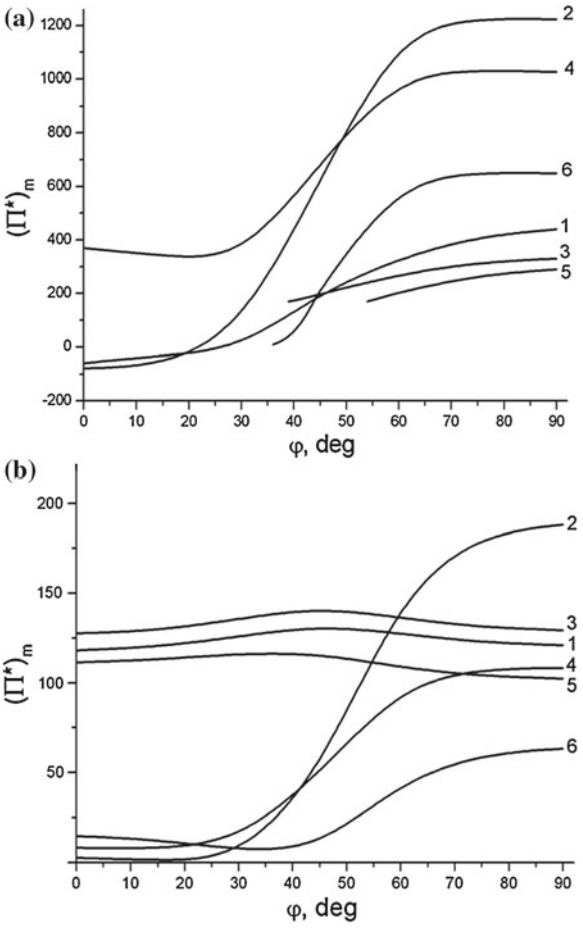

Fig. 3.18 Effective parameters of the 2–2–0 PZN–0.07PT SC / porous elastomer composites with porous P-*k* layers at poroisty $m_p = 0.2$ therein: **a** Local maxima of hydrostatic piezoelectric coefficients $(d_h^*)_m$ (in pC/N, *curves 1*, *3* and *5*) and $(g_h^*)_m$ (in mV·m/N, *curves 2*, *4* and *6*), **b** Local maxima of squared figures of merit $(Q_{33}^*)_m^2$ (in 10^{-11}Pa^{-1}, *curves 1*, *3* and *5*) and $(Q_h^*)_m^2$ (in 10^{-12} Pa^{-1}, *curves 2*, *4* and *6*), **c** Squared figure of merit $(Q_{33}^*)^2$ (in 10^{-11}Pa^{-1}) of the composite with the P-2 layers, and **d** Squared hydrostatic figure of merit $(Q_h^*)^2$ (in 10^{-12}Pa^{-1}) of the composite with the P-2 layers. In graphs *curves 1* and *2* are related to the composite with the P-1 layers, *curves 3* and *4* are related to the composite with the P-2 layers, and *curves 5* and *6* are related to the composite with P-3. In graphs *curves 1*, *2*, *3*, and *4* are related to rotation angles $\varphi = 45°$, 60°, 75°, and 90°, respectively. The rotation mode is shown in inset in Fig. 3.11, and P-*k* layers are schematically represented in insets 2–4 of Fig. 3.17 (reprinted from paper by Krivoruchko and Topolov [30], with permission from IOP Publishing)

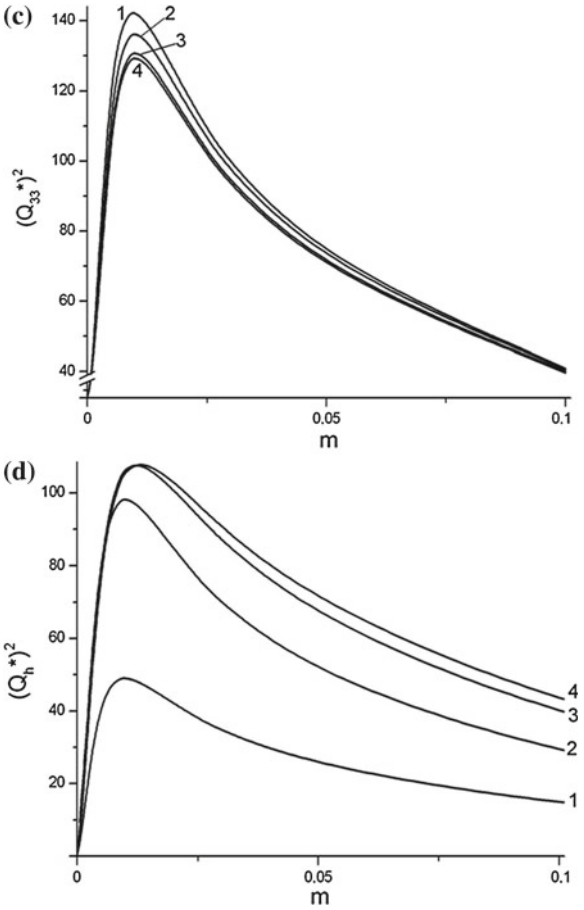

Fig. 3.18 (continued)

3.4 Conclusion

In this Chapter we have discussed the performance of the 2–2-type (laminar) composites based on either FCs or relaxor-ferroelectric SCs. A systematic study of the orientation effects and anisotropic properties has been carried out for the 2–2 and related composites with the following types of the polymer layers: monolithic, auxetic and porous with 3–0 connectivity. The piezoelectric activity and remanent polarisation of ferroelectric polymers has been taken into account. Various orientations of the main crystallographic axes in SCs (single-domain SC poled along $[111]_c$ of the perovskite unit cell and polydomain SC poled along either $[011]_c$ or $[001]_c$ of the perovskite unit cell) have been analysed to study the polarisation orientation effect on the piezoelectric anisotropy and hydrostatic response of the composites.

The anisotropy factors (3.8), (3.9) and (3.22) have been introduced to characterise the piezoelectric response and electromechanical coupling of the 2–2-type composites along the co-ordinate axes. As follows from the results systematised in this chapter, the anisotropy of the piezoelectric coefficients e^*_{3j} and d^*_{3j} and ECFs k^*_{3j} considerably depends on the FC (SC) component and the orientation of the main crystallographic axes in the SC component. In both cases changes in the piezoelectric anisotropy of the FC (SC) component due to the polarisation orientation effect influence the anisotropy factors (3.8), (3.9) and (3.22) in the composite. An additional influence is observed in the presence of the porous or auxetic polymer components with specific ratios of elastic moduli $c^{(2)}_{ab}$. The anisotropy of the piezoelectric coefficients d^*_{3j} is to be taken into consideration at the prediction of the hydrostatic piezoelectric response of the the 2–2-type composites.

The comparative study of the effects of the crystallographic orientation on the performance of the 2–2 SC/polymer composites based on PMN–0.28PT has been carried out for the following poling directions of the SC layers: $[111]_c$ (single-domain state), $[001]_c$ and $[011]_c$ (polydomain states). The effect of the orientation of the main crystallographic axes in the SC component on the hydrostatic parameters (3.2), (3.3), (3.13), and (3.14) has been studied to find maximum values of these parameters for further applications. Of particular interest are large values of the hydrostatic piezoelectric coefficient $e^*_h \approx$(40–45) C/m^2 (Fig. 3.8) in the composite based on the $[111]_c$-poled PMN–0.28PT SC. To a large degree, an increase of e^*_h in comparison to e^*_h of related piezo-active 2–2 composites based on either $[001]_c$- or $[011]_c$-poled SCs is caused by the appreciable elastic anisotropy of the $[111]_c$-poled PMN–0.28PT SC (see Table 3.2).

Conditions (3.25) and (3.26) for the large anisotropy of d^*_{3j} and k^*_{3j} are valid in the SC/auxetic polymer composite, however the simultaneous validity of (3.25) and (3.26) is observed in restricted ranges of the Euler angles and volume fractions of SC (Fig. 3.13). The use of an auxetic polymer as a soft component with the negative Poisson's ratio $\nu^{(n)}$ leads to a considerable hydrostatic piezoelectric response of the composite (Fig. 3.16) even at volume fractions m that are by 5–10 % more than those related to the absolute maximum (minimum) values of the hydrostatic parameters, and this feature is also important for hydrostatic and transducer applications.

In general, data from this chapter enable us to conclude that the performance of the 2–2-type piezo-active composites is highly dependent on the orientation of the main crystallographic axes in SCs effects, and the anisotropy factors change in relatively wide ranges due to the orientation effects.

References

1. Newnham RE, Skinner DP, Cross LE (1978) Connectivity and piezoelectric-pyroelectric composites. Mater Res Bull 13:525–536
2. Topolov VYu, Bowen CR (2009) Electromechanical properties in composites based on ferroelectrics. Springer, London

3. Safari A, Akdogan EK (2006) Rapid prototyping of novel piezoelectric composites. Ferroelectrics 331:153–179
4. Janas VF, Safari A (1995) Overview of fine-scale piezoelectric ceramic/polymer composite processing. J Am Ceram Soc 78:2945–2955
5. Akdogan EK, Allahverdi M, Safari A (2005) Piezoelectric composites for sensor and actuator applications. IEEE Trans Ultrason Ferroelectr Freq Control 52:746–775
6. Huebner W, Reidmeyer MR, Stevenson JW, Busse L (1995) Fabrication of 2–2 connectivity PZT / thermoplastic composites for high efficiency linear arrays. In: Pandey RK, Liu M, Safari A (eds) ISAF'94: Proceedings of the 9th IEEE International symposium on applications of ferroelectrics, University Park, Pennsylvania, 7–10 Aug 1994. IEEE, Piscataway, pp 206–209
7. Zhang QM, Geng X (1994) Dynamic modeling of piezoceramic polymer composite with 2–2 connectivity. J Appl Phys 76:6014–6016
8. Getman IP, Ryabov AP, Ustinov YuA (1987) On possibilities of the averaging method in a task on propagation of waves in an electroelastic layer with a periodic thickness inhomogeneity. Izvestiya Akademii Nauk SSSR. Mekhanika Tverdogo Tela 3:118–124 (in Russian)
9. Khoroshun LP, Maslov BP, Leshchenko PV (1989) Prediction of effective properties of piezoactive composite materials. Naukova Dumka, Kiev (in Russian)
10. Cao W, Zhang QM, Cross LE (1993) Theoretical study on the static performance of piezoelectric ceramic-polymer composites with 2–2 connectivity. IEEE Trans Ultrason Ferroelectr Freq Control 40:103–109
11. Grekov AA, Kramarov SO, Kuprienko AA (1987) Anomalous behavior of the two-phase lamellar piezoelectric texture. Ferroelectrics 76:43–48
12. Hashimoto KY, Yamaguchi M (1986) Elastic, piezoelectric and dielectric properties of composite materials. In: Proceedings of IEEE Ultrasonic Symposium, 17–19 Nov 1986. Williamsburg, New York, pp 697–702
13. Turcu S, Jadidian B, Danforth SC, Safari A (2002) Piezoelectric properties of novel oriented ceramic-polymer composites with 2–2 and 3–3 connectivity. J Electroceram 9:165–171
14. Levassort F, Lethiecq M, Millar C, Pourcelot L (1998) Modeling of highly loaded 0–3 piezoelectric composites using a matrix method. IEEE Trans Ultrason Ferroelectr Freq Control 45:1497–1505
15. Gibiansky LV, Torquato S (1997) On the use of homogenization theory to design optimal piezocomposites for hydrophone applications. J Mech Phys Solids 45:689–708
16. Grekov AA, Kramarov SO, Kuprienko AA (1989) Effective properties of a transversely isotropic piezoelectric composite with cylindrical inclusions. Mech Compos Mater Struct 25:54–61
17. Turik AV, Topolov VYu (1997) Ferroelectric ceramics with a large piezoelectric anisotropy. J Phys D Appl Phys 30:1541–1549
18. Zhang R, Jiang B, Cao W (2003) Single-domain properties of $0.67Pb(Mg_{1/3}Nb_{2/3})O_3 - 0.33PbTiO_3$ single crystals under electric field bias. Appl Phys Lett 82:787–789
19. Zhang R, Jiang B, Cao W (2003) Orientation dependence of piezoelectric properties of single domain $0.67Pb(Mn_{1/3}Nb_{2/3})O_3 - 0.33PbTiO_3$ crystals. Appl Phys Lett 82:3737–3739
20. Noheda B (2002) Structure and high-piezoelectricity in lead oxide solid solutions. Curr Opin Solid State Mater Sci 6:27–34
21. Topolov VYu (2004) The remarkable orientation and concentration dependences of the electromechanical properties of $0.67Pb(Mg_{1/3}Nb_{2/3})O_3 - 0.33PbTiO_3$ single crystals. J Phys Condens Matter 16:2115–2128
22. Liu G, Jiang W, Zhu J, Cao W (2011) Electromechanical properties and anisotropy of single- and multi-domain $0.72Pb(Mg_{1/3}Nb_{2/3})O_3 - 0.33PbTiO_3$ single crystals. Appl Phys Lett 99:162901–3P
23. Zhang R, Jiang B, Jiang W, Cao W (2006) Complete set of elastic, dielectric, and piezoelectric coefficents of $0.93Pb(Zn_{1/3}Nb_{2/3})O_3 - 0.33PbTiO_3$ single crystal poled along [011]. Appl Phys Lett 89:242908 (3 pp.)
24. Sessler GM (1981) Piezoelectricity in polyvinylidenefluoride. J Acoust Soc Am 70:1596–1608

25. Kar-Gupta R, Venkatesh TA (2007) Electromechanical response of 1–3 piezoelectric composites: an analytical model. Acta Mater 55:1093–1108
26. Topolov VYu, Krivoruchko AV (2009) Polarization orientation effect and combination of electromechanical properties in advanced $0.67Pb(Mg_{1/3}Nb_{2/3})O_3 - 0.33PbTiO_3$ single crystal/polymer composites with 2–2 connectivity. Smart Mater Struct 18:065011 (11 pp.)
27. Newnham RE (1994) Nonmechanical properties of composites. In: Kelly A, Cahn RW, Bever MB (eds) Concise encyclopedia of composite materials. Elsevier, Oxford, pp 214–220
28. Berlincourt DA, Cerran DR, Jaffe H (1964) Piezoelectric and piezomagnetic materials and their function in transducers. In: Mason W (ed) Physical acoustics. Principles and methods. Methods and devices, vol 1. Pt A. Academic Press, New York, London, pp 169–270
29. Topolov VYu, Krivoruchko AV, Bowen CR, Panich AA (2010) Hydrostatic piezoelectric coefficients of the 2–2 composite based on [011]-poled $0.71Pb(Mg_{1/3}Nb_{2/3})O_3 - 0.33PbTiO_3$single crystals. Ferroelectrics 400:410–416
30. Krivoruchko AV, Topolov VYu (2007) On the remarkable performance of novel 2–2-type composites based on [011] poled $0.93Pb(Zn_{1/3}Nb_{2/3})O_3 - 0.33PbTiO_3$ single crystals. J Phys D Appl Phys 40:7113–7120
31. Topolov VYu, Krivoruchko AV (2009) Orientation effects in 2–2 piezocomposites based on $(1-x)Pb(A_{1/3}Nb_{2/3})O_3 - xPbTiO_3$ single crystals (A = Mg or Zn). J Appl Phys 105:074105 (7 pp.)
32. Topolov VYu, Glushanin SV (2002) Evolution of connectivity patterns and links between interfaces and piezoelectric properties of two-component composites. J Phys D Appl Phys 35:2008–2014
33. Evans KE, Alderson KL (1992) The static and dynamic moduli of auxetic microporous polyethylene. J Mater Sci Lett 11:1721–1724
34. Sun E, Cao W, Jiang W, Han P (2011) Complete set of material properties of single domain $0.24Pb(In_{1/2}Nb_{1/2})O_3$-$0.49Pb(Mg_{1/3}Nb_{2/3})O_3 - 0.33PbTiO_3$ single crystal and the orientation effects. Appl Phys Lett 99:032901 (3 pp.)
35. Zhang S, Liu G, Jiang W, Luo J, Cao W, Shrout TR (2011) Characterization of single domain $Pb(In_{0.5}Nb_{0.5})O_3$-$Pb(Mg_{1/3}Nb_{2/3})O_3 - 0.33PbTiO_3$ crystals with monoclinic phase. J Appl Phys 110:064108 (5 pp.)
36. Topolov VYu, Krivoruchko AV, Bowen CR (2012) Anisotropy of electromechanical properties and hydrostatic response of advanced 2–2-type composites. Phys Status Solidi A 209:1334–1342
37. Dunn M (1995) Effects of grain shape anisotropy, porosity, and microcracks on the elastic and dielectric constants of polycrystalline piezoelectric ceramics. J Appl Phys 78:1533–1541
38. Dunn ML, Taya M (1993) Electromechanical properties of porous piezoelectric ceramics. J Am Ceram Soc 76:1697–1706